AN ABSTRACT OF THE THESIS OF

ANA MACARIO for the degree of MASTER OF SCIENCE in GEOPHYSICS

presented on JULY 28, 1989.

Title : FREQUENCY RESPONSE FUNCTION ANALYSIS OF THE EQUATORIAL MARGIN OF BRAZIL USING GRAVITY AND BATHYMETRY

Abstract approved : Redacted for Privacy

Richard W. Couch

Redacted for Privacy

J. Paul Dauphin

The overall objective of this study is to address questions concerning the long-term mechanical strength of the lithosphere across the equatorial margin of Brazil. The approach used in this study consists of calculating the frequency response function estimates, also called admittance, using gravity and bathymetry data. These experimental estimates are then compared to theoretical admittance curves for Airy and thin elastic plate models for which estimates on the flexural rigidity or, equivalently, effective elastic thickness may be made.

Twelve profiles, each 256 km long, were extracted from gridded gravity and bathymetry data (data sources: project EQUANT, Defense Mapping Agency, National Geophysical Data Center files and GEOS 3/SEASAT altimeter data). Three profiles were specifically used for testing truncation errors introduced by four different data treatment procedures (before Fourier transforming the data) : detrending, applying 10% cosine tapering, mirror imaging and the use of the first derivatives. The method I

adopted is similar to the one used by McNutt (1983) and consists of testing how reliably a given admittance estimate can be recovered as a function of the data treatment procedure. A "predicted" gravity anomaly was obtained by convolving each bathymetric profile with a theoretical admittance filter. The edges of this anomaly are then submitted to the same treatment as the corresponding bathymetric profile before Fourier transforming both profiles and calculating admittance. The stability of the long-wavelength admittance estimates, in the presence of noise, was also investigated by introducing Gaussian noise, in the range of -50 to +50 mGals, in the "predicted" gravity signal. The results indicate that relatively unbiased long-wavelength admittance estimates can be obtained by using the first derivative of the data sets. In addition, it is shown that the mirroring technique, used in previous admittance studies across Atlantic-type margins, leads to overestimated admittance values and, therefore, overestimated flexural rigidities.

Neither the theoretical curves for the Airy model nor the plate flexure model can explain the experimental admittance estimates. Not only are the experimental admittance estimates higher than the predicted values but they also have a narrower peak than the theoretical curves. This raises the question of the applicability of highly simplified isostatic models for tectonic provinces such as Atlantic-type continental margins. The following reasons may explain the discrepancies between the experimental and theoretical admittance estimates :

(1) The abrupt nature of the transition between oceanic and continental crust controlled by the Romanche Fracture Zone - Unlike the eastern North American continental margin which was formed as a result of extensive rifting and pulling apart, the obliquely-rifted equatorial margin of Brazil has undergone a complex tectonic evolutionary process, where additional components such as shear and right-lateral

wrenching were present. Therefore, representing the margin as a thin homogeneous elastic plate might be reasonable when the transition is gradual (for which the uniform flexural rigidity assumption seems reasonable) but is probably not a good approximation when it is as abrupt as the equatorial margin of Brazil .

(2) Presence of subsurface loads - Previous studies have shown that estimates of the average flexural rigidity of continental lithosphere using the admittance approach are biased when subsurface loads are present. In principle, the proximity of the Romanche Fracture Zone and associated volcanism suggest that shalow buried loads, caused by intrusive bodies, might be present in the area. This could partially account for the mismatch between theoretical curves and experimental admittance estimates.

(3) "Masked" estimates - The admittance estimates presented here are likely to reflect the combination of two different signals : one related to the compensation of the Barreirinhas/Piaui-Camocim sub-basin which has no topographic/bathymetric expression and the other one related to the topography/bathymetry and its compensation which is of interest in the admittance studies. Since the wavelengths of these signals do not differ by much (around 80-100 km for the basin) it is possible that in the averaging process some overlaping occurs. The combination of these signals could yield anomalous results masking the admittance estimates in the diagnostic waveband.

In addition, I present a two-dimensional cross section obtained by forward modelling the gravity anomaly along a profile using the line integral method. The uniform sedimentary infill of the Barreirinhas/Piaui-Camocim basin basin is enough to account for the gravity low over the inner shelf and no Moho topography is required. A plausible explanation for this "rootless" basin structure is that the lithosphere is capable of supporting the sediment infill load , and thus, has finite flexural rigidity (basin is locally uncompensated).

Frequency Response Function Analysis of the Equatorial Margin of Brazil Using Gravity and Bathymetry

by

Ana L. G. Macario

A THESIS

submitted to

Oregon State University

in partial fulfillment of the requirements for

the degree of

Master of Science

Completed on July 28, 1989

Commencement June 1990

APPROVAL :

Redacted for Privacy

Associate Professor of Geophysics in charge of major

Redacted for Privacy

Research Associate of Geophysics in charge of major

Redacted for Privacy

Dean of College of Oceanography

Redacted for Privacy

Dean of Graduate School

Date thesis is presented: July 28, 1989

Typed by : Ana L. G. Macario

ACKNOWLEDGEMENTS

I would first like to thank my parents, Victor and Alice Macario without whom none of this would have ever happened. I am very thankful for all their intense love, dedication and immense support since my very first years in school.

I am also very thankful to my advisor and friend Dr. J. Paul Dauphin for his support, dynamism and encouragement through the tough times. The fact that he was willing to take me as his student after Dr. Couch's illness (my previous advisor) and that he had always truly valued my research project made my experience at O.S.U. very special. His sincere enthusiasm and lively discussions frequently joined by Dr. Gordon E. Ness were greatly appreciated. Ness' outgoing and charming personality and great sharp sense of humor have added a lot of spice to the dull portions of my research. I really appreciated the opportunity of participating in the EQUANT '87 cruise shortly after arriving at O.S.U. In spite of getting "docksick", I learned a lot about geophysical instrumentation and ARGO and satellite navigation. Both Dauphin and Ness turned out to be very special dear friends with whom I shared the best moments in Oregon not to mention the great times at A.G.U. meetings in San Fransisco. They also provided the moral support which has helped me building up the self confidence that I will need to pursue my PhD program at Lamont-Doherty Geological Observatory of Columbia University.

My thanks go to Dr. Richard W. Couch who I had as my academic advisor in the first year. I also want to thank Dr. Robert Hollmann and Dr. Nick Pisias for helping me with some theoretical concepts in the very first beginning of my thesis. And of course, a very special thanks to my minor professor from the Department of Mathematics, Dr. Joel Davis, who is a marvelous teacher . Being his student for three consecutive terms in Numerical Analysis was a very enriching experience. He has taught me a series of subtleties and "catches" in the subject as well as to be critical with printing matter.

My special thanks also go out to Michael Kelsay, the computer system manager at CONMAR. I will never forget his kindness in helping me inumerous times with software and hardware "bugs" and making extra "room" for my gridding files. He was always around willing to help me when I was in panic.

Next come my classmates at O.S.U. with whom I have enthusiastically discussed some of the aspects of my research : Luis Braga, Juan Garcia, Rainer Ludwig and John Rees. A special thanks goes to Pierre Douguin, an ex-student at O.S.U. who seems to know Macintonshes and good wines (a true Frenchman !) as no one else. Thanks for "rescuing" me after several power failures during the very last part of writing my thesis.

My sincere appreciation also goes to Gloria Walker who has helped in one way or another during my stay here. She's been like a "mom" to me, very much supportive at all times in her own way. I am also very thankful to Steve Troseth for nicely drafting some of the figures that went into my thesis and giving me helpful hints concerning cycling.

Last, but not least, a truly special thanks to a great friend Anne Yeaple for helping me with my figures for A.G.U. and for all the companionship, support and encouragement she has given me since my very first day in Corvallis. She became a very dear heart sister to me, getting me interested in sports and learning about my inner self.

This study is part of a cooperative project involving the Continental Margin Study Group (CONMAR) at Oregon State University and PETROBRAS, a Brazilian oil company. I am grateful to Dr. Marco Polo Pereira da Boa Hora, chief of the potential field sector at PETROBRAS for his encouragement to apply to O.S.U. He has also provided much of the support for the realization of the EQUANT project. I would like to thank PETROBRAS specifically for the release of seismic reflection profiles and bore-hole data. Renato Kowsmann from PETROBRAS/CENPES has also provided very helpful comments. This study was supported by a grant from the Office of Naval Research (O.N.R.) N 00014-84-C-0673.

TABLE OF CONTENTS

LIST OF FIGURES

LIST OF APPENDICES FIGURES

LIST OF TABLES

FREQUENCY RESPONSE FUNCTION ANALYSIS OF THE EQUATORIAL MARGIN OF BRAZIL USING GRAVITY AND BATHYMETRY

1 - INTRODUCTION AND PREVIOUS WORK

A number of recent studies have addressed the mechanical properties of the lithosphere for Atlantic-type margins by analysis of the free-air gravity anomalies (Karner and Watts, 1982; Watts and Thorne, 1984; Watts, 1988; Thorne and Watts, 1989). Karner and Watts (1982), for instance, used the isostatic response function theory originally developed by Dorman and Lewis (1970), to study passive margins . The response or admittance function approach assumes that gravity anomalies result from the summing effect of topography and its compensation and consists of finding a function which, when convolved with topography/bathymetry, reproduces these anomalies. The experimental admittance function, calculated as the ratio of the Fourier transforms of gravity and bathymetry, may then be compared to the admittance predicted by simple isostatic models from which estimates for the flexural rigidity of the lithosphere or, equivalently, effective elastic thickness are infered. The term "effective" elastic thickness is used in this study to denote that part of the seismo-thermal lithosphere on which elastic stress can be maintained over geological times. Values for the flexural thickness of the lithosphere are substantially less than the thermal-seimological thickness (invariably less than half) since these record the response to short term loads (Cochran, 1980; Watts, 1981).

Karner and Watts (1982) used the admittance approach to describe the mechanical behaviour of stretched continental lithosphere under sedimentary load. The resulting admittance function for three passive margins of different thermal ages (eastern North America, southwest Africa and Coral Sea/Lord Howe Rise) were interpreted in terms of an

elastic continuous plate model in which the long-term mechanical strength of the lithosphere increases with age. Their estimates are similar to the ones obtained for mid-ocean ridge crests and, therefore, significantly smaller than those deduced for old oceanic lithosphere (figure 1). These results are attributed to the intense heat at the margins during rifting. For the U.S Atlantic margin, Karner and Watts (1982) suggest an effective elastic thickness of 10-20 km. Their results are not in agreement with Watts (1988) who concluded that the stretched continental lithosphere of the Baltimore Canyon Trough has not acquired any significant strength after extension, that is, the approximately 15 km of sediments are locally supported by the lithosphere. However, G. D. Karner (personnal communication) argues that the low estimates for the flexural rigidities obtained by Watts (1988) are biased towards a low value since a local isostatic model was used to reconstruct the crustal structure of the margin . Also, the presence of a thick sediment pile can significantly change the thermal structure of the lithosphere accounting, therefore, for the low flexural rigidity values . Diament et al. (1986) also examined the isostatic compensation of the northern Bay of Biscay continental margin using the admittance function approach. They interpreted the experimental admittance estimates in terms of two different processes: local compensation (Airy model with a crustal thickness of 20 km) for wavelengths greater than 250 km and regional compensation for shorter wavelengths (plate model with an effective elastic thickness of 8 km).

The overall objective of this study is to address questions concerning the mechanical strength of the lithosphere across the equatorial margin of Brazil. Since the geophysical information available is primarily gravity and bathymetric data, and the crustal structure and loading history cannot be adequately constrained for backstripping purposes, the admittance approach is used. The rationale for obtaining experimental admittance estimates is to be able to interpret them in terms of simple isostatic models and determine which, if any, of the models can account for the experimental results. Additional analyses

include forward modelling and the downward continuation of the residual isostatic gravity anomalies.

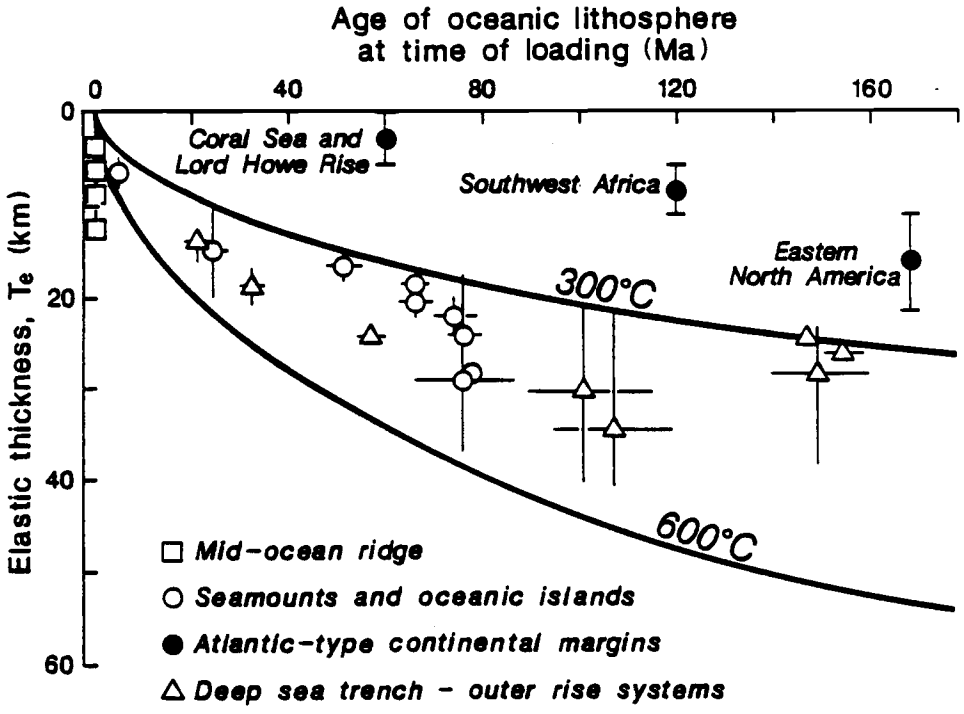

Figure 1 - Effective elastic thickness of oceanic lithosphere as a function of its age at the time of loading for several tectonic provinces (after Watts et al., 1980; Karner and Watts, 1982). The 300º and 600º C isotherms based on the cooling plate model (Parsons and Sclater, 1977) are represented by solid lines. The simplest interpretation of the results is that oceanic lithosphere becomes more rigid in its response to surface loads as it cools and thickens with age. The elastic thickness for each estimates was obtained assuming Young's modulus $E = 10^{11}$ kg m^{-1} s^{-2} and Poisson's ratio $\upsilon = 0.25$

2 - TECTONIC AND GEOLOGIC FRAMEWORK

The study area comprises the eastern part of the obliquely-rifted equatorial margin of Brazil situated between latitudes 5°30' S - 1° N and longitudes 44°45' º W - 34° 45' W. Figure 2 shows the main physiographic provinces within the area. Several Mesozoic marginal basins occur within the area which are the subject of intense research interest for their potential hydrocarbon resources. The only onshore basin within the area is the Barreirinhas basin. The offshore basins are, from west to east : Ceara, sub-divided into Piaui-Camocim, Acarau and Mundau, and Potiguar.

The depocenter of the onshore Barreirinhas basin trends approximately WNW/ESE and is bounded to the south by the Ferrer-Urbano Santos Arch (Gorini, 1981; Zalan and Warme, 1985). In the offshore region, the basin depocenter changes to an EW direction which is in line with the depocenter of the Piaui-Camocim basin located to the east. The sediment infill along the EW depocenter of both basins is estimated to around than 6 km (Gorini, 1981; Azevedo, 1986). It consists mainly of course, non-marine, terrigenous sediments eroded from the Ferrer-Urbano Santos Arch and Para-Maranhao platform (outside the studied area) overlapped by transitional to marine post-rift sediments. The Barreirinhas and Piaui-Camocim basins are separated by an anticlinal structural high, the Tutoia high. Previous studies suggested that the high was originally a depocenter which, under transpression, was transformed into an inversion structure. The Barreirinhas and Piaui basins are treated here as one tectonic/sedimentary unit outlined by the rhombohedral shaped graben shown on the gravity map (figure 3) and referred to as the Barreirinhas/Piaui-Camocim basin.

The Ceara High separates the Piaui-Camocim basin from the Acarau basin. An approximately linear feature, called the Transversal Lineament, trending NNE/SSW, roughly separates Acarau basin from the Mundau basin. The Piaui-Camocim, Acarau and Mundau basins are bounded to the north by an offshore high, the Atlantic High, and to the south by the Parnaiba Platform, a shallow Precambriam basement, which corresponds to an eastward extension of the Ferrer-Urbano Santos Arch (Gorini, 1981; Zalan and Warme, 1985) . This platform, which crops out near the coast is covered by a thin sediment layer less than 1 km thick as shown in seismic profile AA' (figures 3 and 4). The Atlantic High defines the axis of a transpressive belt where maximum shear stress and transpressional uplift is believed to have occurred according to Zalan and Warme (1985). The elongation (N80-90E) and position of the high corresponds exactly to the axis of the Romanche Fracture Zone. Seismic data indicate that the Atlantic High is comprised of several blocks such as horsts and grabens, anticlines and synclines and reversed and normal faults (Zalan and Warme, 1985). Well data (CES-97) from the top of the Ceara High (figure 2) indicates an acid volcanic intrusive complex composed of ryolitic lava flows, volcanic breccias, minor granitic intrusions, pyroclastic beds, dykes and predominantly clastic conglomerates and breccias (Zalan and Warme, 1985). In summary, well and seismic data support the idea that the Atlantic and Ceara Highs are the resilt ofto strike-slip volcanism representing a westward extension of the Romanche Fracture Zone.

Another structural high, the Fortaleza high, separates the Mundau basin from the Potiguar basin, which is bounded to the north by the Fernando de Noronha Fracture Zone. The sediment infill of the offshore Potiguar basin does not exceed 3000 m and its structure is a result of the reactivation of old structural trends present in the Precambrian shield and the development of new structural trends at high angles to the Precambrian shield (Gorini, 1981; Francolin and Szatmari, 1987; Szatmari et al., 1987). A structural high called Touros High is situated at the edge of the margin (figure 2).

The North Brazilian Ridge consists of a series of aligned seamounts roughly parallel to the shoreline with a sediment cover of 2-3 km (Houtz et al, 1977; Kumar et al, 1974) that separates the continental rise from the Ceara abyssal plain. It is composed of 3 segments, two of them extending westward of the Saint Paul's Fracture Zone and the Romanche Fracture Zone and the other one trending NW-SE and believed to be part of an abandoned spreading center (LePichon and Hayes, 1971; Gorini, 1981). Figure 5 shows a composite section across the NW-SE segment of the North Brazilian Ridge based on two-ship refraction results (Houtz et. al., 1977).

Another important feature present in the area is a relatively large flat-topped seamount, the Ceara Guyot. It is at least 100 Ma old and probably a result of volcanism along the Romance Fracture Zone (Costa and Kowsmann, 1981; Lobo, 1987). Dredge hauls along the northeast flank of the Ceara guyot recovered calcareous sediments rich in phosphorous at a depth of 700 meters. According to Costa and Kowsmann (1981), the sediments were deposited at depths of less than 150 m during the Late-Middle Miocene implying subsidence rates on the order of 0.04 mm/yr. DSDP borehole information obtained for the Northern Brazilian Ridge yield subsidence rates which are twice as fast (Gorini, 1981).

The obliquely-rifted equatorial margin of Brazil has an atypical tectonic setting which developed as a result of a complex sequence of events. The occurrence of folds and reverse faults in some of the marginal basins was first reported by Miura and Barbosa (1972). These compressional features, obviously anomalous in the context of passive margins, occur mainly across the Barreirinhas/Piaui-Camocim basin. A recent detailed structural analysis was done by Zalan and Warme (1985) on the Piaui-Camocim basin, based on seismic sections, well information, aeromagnetic data and Landsat satellite images of the coastal region. This study suggested that the evolution of this particular basin can be explained in terms of two distinct tectonic events : the first event is the rift stage, which

marks the beginning of the NS separation between South America and Brazil (early Alagoas; similar to Aptian) . The basin started developing through a series of normal faults. Then around 98-95 Ma, the separation changed from NS to EW along the Romanche Fracture Zone and right-lateral convergent wrenching predominated. As a consequence, the normal faults created in the rift stage were reactivated as right-lateral strike-slip faults forming synthetic and antithetic strike slip faults, flower structures, enchelon fold and shale ridges.

The admittance technique in this study focuses on the westernmost part of the study area, specifically the Barreirinhas/Piaui-Camocim depositional system. The main reasons for this choice were:

(1) That part of the margin contains the bulk of the compressional features related to the combination of rifting and wrenching tectonism; therefore, I expect the estimates for the apparent flexural strength of the lithosphere to be the most representative for the margin since rifting.

(2) The Barreirinhas/Piaui-Camocim depocenter has the deepest sediment accumulation (over 6 km) and therefore the admittance estimates for the area should reflect the mechanical response of the lithosphere to the sedimentary load.

(3) The elongated configuration of the EW trending features paralleling the west part of the equatorial margin allows application of admittance analysis along profiles oriented perpendicular to the main structure. However, this type of analysis is probably not well suited for the eastern portion of the study area because of the 3-dimensional nature of the features found in this area (figure 2), e.g., the Ceara Guyot).

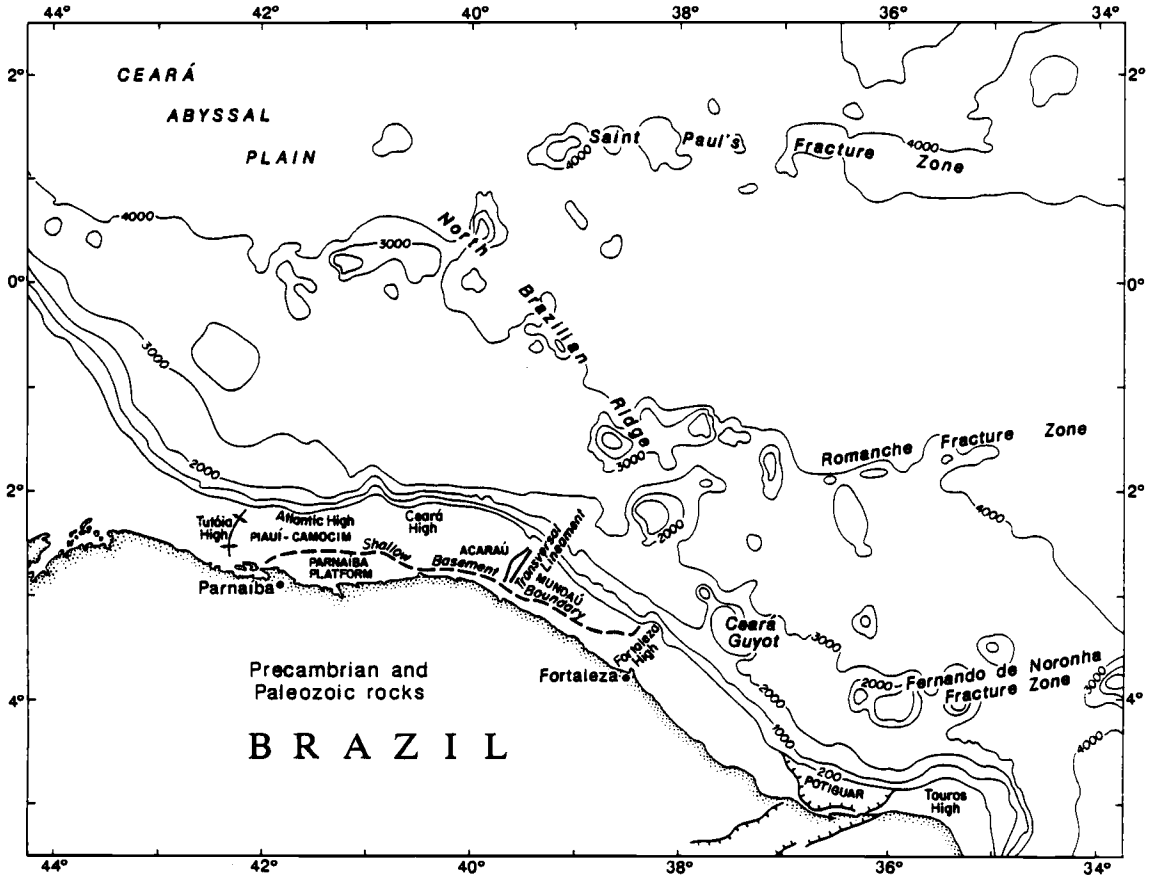

Figure 2 - Simplified map showing the main structural and physiographic features in the study area.

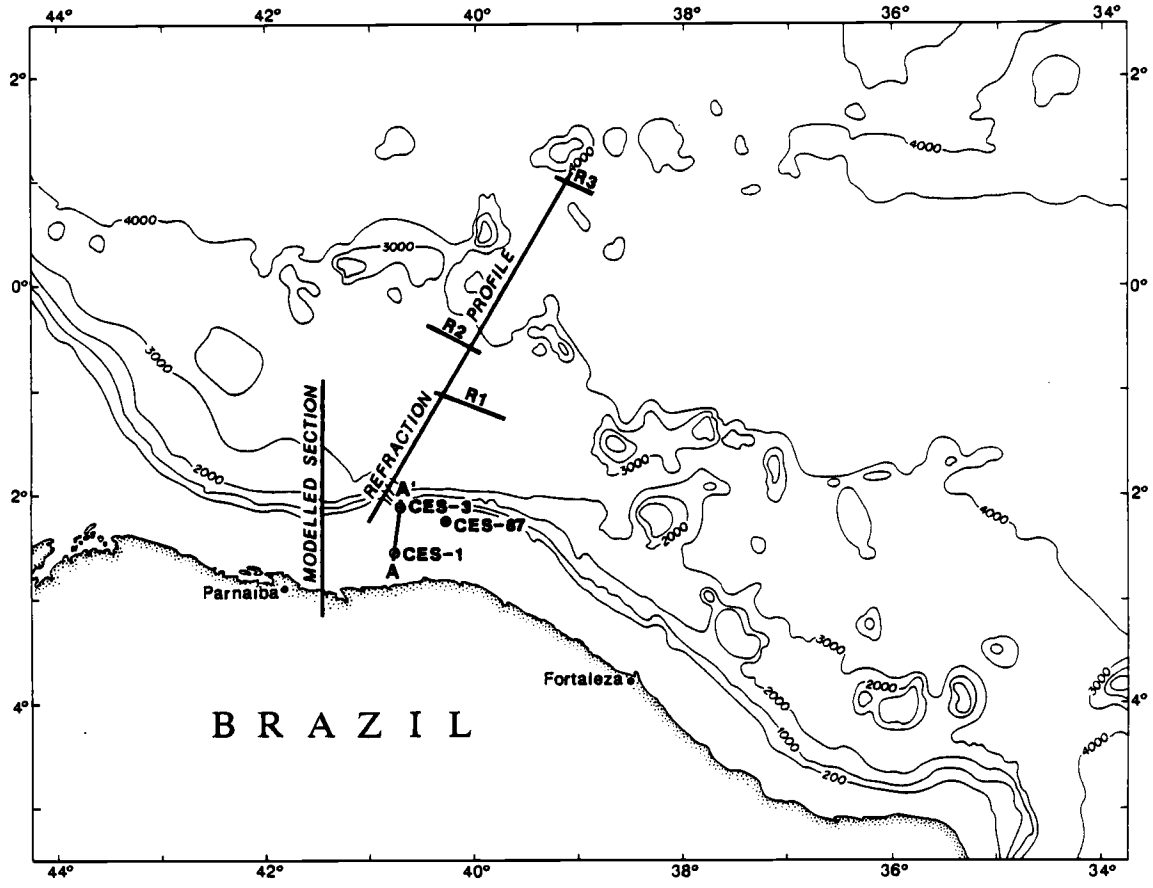

Figure 3 - Map showing location of: seismic reflection AA', refraction profiles R_1, R_2 and R_3, modelled cross section, boreholes CES-1, CES-3 and CES-87 and cross section by Houtz et al. (1977) using seismic refraction data (shown in figure 5).

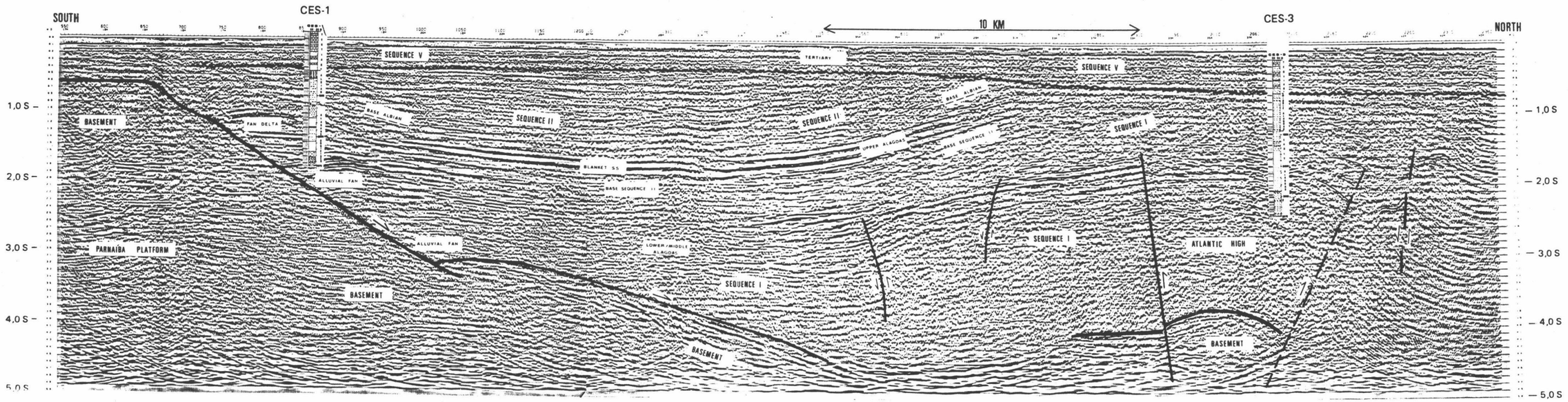

Figure 4 - Migrated time section AA'. Figure 3 shows the location of this seismic line and boreholes CES1 and CES3. The top of the Parnaiba basement reflector (from Zalan and Warme, 1985) was used to constrain the gravity model presented in figure 22.

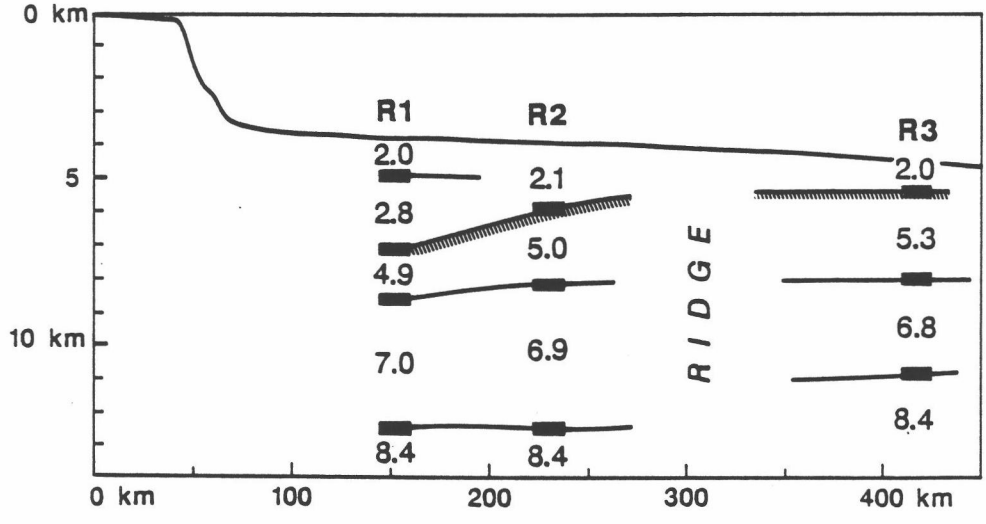

Figure 5 - Crustal structure based on two-ship seismic refraction solutions across the NW-SE segment of the North Brazilian Ridge (after Houtz et al., 1977). The top of oceanic layer 2 is indicated by hatching. Section location is shown in figure 3.

3 - DATA BASE

The gravity and bathymetric maps shown in figure 6 and 7 were produced using the following data sources: project EQUANT (the 1987 cruise Equant I), data files obtained from the Defense Mapping Agency (DMA) and the National Geophysical Data Center (NGDC) and a combination of GEOS3/SEASAT altimeter data. The main data set, Equant I, covers the Eastern part of the equatorial margin of Brazil to water depths of 2800 meters; a combination of DMA, NGDC and altimeter data were used for the adjacent areas. A general description of all data sources as well as the details concerning data acquisition and reduction of Equant I are presented below.

(1) EQUANT I - The data were acquired in 1987 (first part of project EQUANT), by CONMAR (The Continental Margin Study Group) at Oregon State University, with the technical and scientific support of PETROBRAS, the Brazilian oil company. A total of 7916 nautical miles of bathymetric, magnetic and gravimetric data were collected with trackline spacings of ~ 9 km for legs 1, 2 and 3 and ~ 14 km for leg 4.

Navigation

The navigation for Equant I was 90 % based upon an ARGO shore-based pseudo range-range transponder system supplemented with Transit and GPS satellite positioning. Magnavox MX 1502 geocievers were used to geodetically locate the shore-based transponders. ARGO, which is a phase comparison, lane counting system, provided 30 second position determinations for individual fixes within a lane precise to about 10 meters. Its maximum operational range is approximately 400 nautical miles during the day and 150 nautical miles at night due to an increase in the skywave/groundwave signal ratio.

Tracklines more distant from shore were navigated using Transit and GPS. Estimated position accuracy was ~120 meters for GPS and ~300 meters for Transit.

In order to obtain a uniform sequence of positions in time, a bi-cubic spline was used to interpolate the station locations and a filter was then applied to the data . The velocities used in the Eotvos corrections were computed over a 30-second navigation interval using the distance between station locations divided by the elapsed time between positions. The average ship velocity was 9 knots.

Bathymetry

A 12 khz Raytheon PTR-105B transceiver and a Raytheon LSR-1807M recorder were used to register bathymetry. The analog data were digitized at 1 minute intervals in fathoms of depth. Depths were converted from two-way travel times using a constant sound-speed in the water of 800 fathoms/sec and corrected using the tables by Carter (1980). No filtering was applied to the bathymetric data. The estimated rms uncertainties obtained by analysis of 203 crossings is 25.2 meters.

Gravity

The gravity data were collected using the LaCoste & Romberg surface ship gravity meter S-42 mounted on a 2-axis gyro stabilized platform. This gravity meter applies a 10 minute symmetrical filter to the gravity values, originally recorded at every 10 seconds, to remove ship motion accelerations from the data. Two LaCoste & Romberg land gravity meters were used to calculate the meter drift from repeated measurements on the IGSN-71 referenced base at the Port of Fortaleza. The gravity values were re-sampled at every 3 minutes and Eotvos corrected using the information supplied by the navigation files.

The free-air gravity anomalies were obtained by subtracting the theoretical gravity values, computed using the formula adopted by the International Association of Geodesy

GRS-67 System, from the observed values. Based on 287 crossings, the estimated rms uncertainty in the free-air gravity values is 2.98 mGals.

(2) OTHER SHIPBORNE GRAVITY/BATHYMETRY DATA - Data were obtained from the Defense Mapping Agency (DMA) and the National Geophysical Data Center (NGDC). The gravity data sets collected prior to 1953 using only celestial navigation were not included. Because DMA files contain data of varying quality, no network adjustment was attempted. Instead, trackline crossings were visually inspected; bad data points were omitted and corrections added to some tracklines when necessary to reduce the data to the same GRS-67 system.

The bathymetry data sets were of uniform quality although some individual tracklines were not used. A five-minute digital data grid ETOPO5 was used to "monitor" some of the bathymetric features and "fill" some areas where the trackline coverage was sparse. The rms error is estimated to be at least of 11 mGals for gravity and 42 meters for bathymetry (based on 20 random crossings).

(3) LAND GRAVITY/TOPOGRAPHY DATA- Proprietary Bouguer land gravity measurements and respective elevations were obtained for the westernmost part of the studied area (Blitzkow, Universidade de Sao Paulo/ USP). The non-uniform distribution of these values is shown in figure 6 as small dots on land.

(3) SATELLITE ALTIMETER DATA - For oceanic areas outside the Equant I area where the gravity tracklines were sparse, I used the free-air gravity anomalies derived from a combined GEOS3/SEASAT altimetry data set. These data and their respective standard deviations are part of a 7.5' world wide grid produced by R. H. Rapp at Ohio State University. According to Rapp (1986), the resolution of the gravity anomalies is around 21 km and agreement with shipborne gravity are on the order of $\pm$ 10 to 30 mGals

is expected. The data integration was done only for areas where the standard deviation was less than 20 mGals.

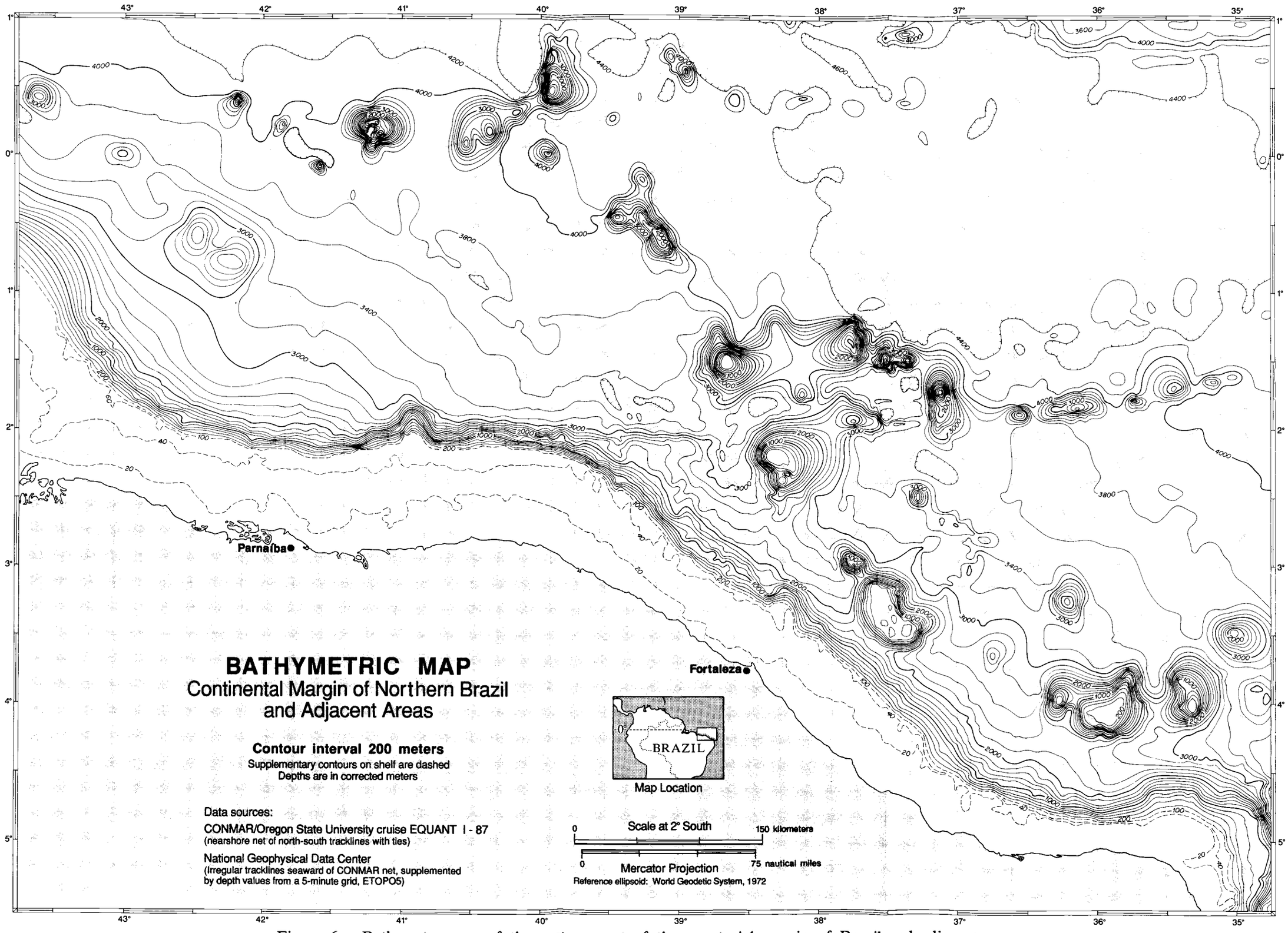

Figure 6 – Bathymetry map of the eastern part of the equatorial margin of Brazil and adjacent areas.

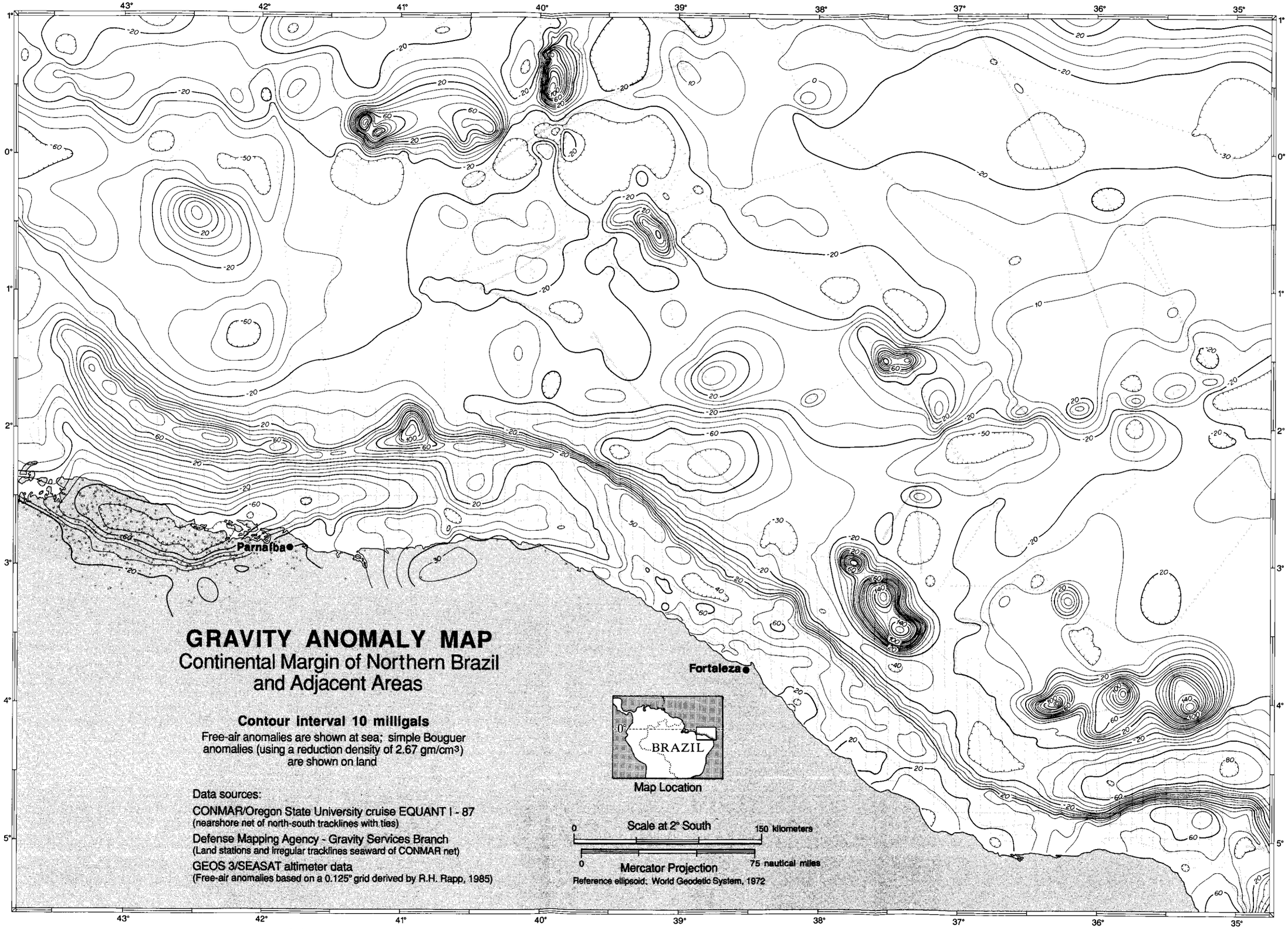

Figure 7 – Gravity map of the eastern part of the equatorial margin of Brazil and adjacent areas.

4- GRAVITY AND BATHYMETRIC MAPS

Figures 6 and 7 show the gravity and bathymetry contour maps constructed using the above mentioned data base. These maps were generated using a minimum curvature technique (Briggs, 1974) applied iteratively from a coarse to a fine grid, resulting in a final grid spacing of 1 nautical mile. The tracklines are shown as dotted lines.

The bathymetry map was contoured at 200 m intervals; for depths shalower than 200 m, contour intervals of 20 m were used . The main structural and sedimentary features have been identified on the bathymetry map . The western part of the study area has an approximately EW trend and is characterized by a broad continental shelf with widths ranging between 90-120 km. The continental slope is relatively steep (8-10 degrees) and the shallowest feature is the Ceara High which separates the Piaui-Camocim and Acarau basins. A much narrower shelf (50-80 km) trending NW-SE with a gentler slope (5-7 degree) characterizes the eastern part of the equatorial Brazilian margin. The Ceara guyot, oriented approximately parallel to this portion of the margin rises to water depths as shallow as 200 meters, representing the shallowest structural high present in the studied area. The deepest bathymetric feature is the Ceara Abyssal Plain where water depths on the order of 5000 m occur.

The gravity map shown in figure 6 was contoured at 10 mGal intervals using simple Bouguer gravity values on land and free-air gravity values at sea. The free-air gravity anomaly "edge effect" associated with passive margins is well developed in the westernmost part of the studied area. It is marked by the presence of a sharp high of about +90 to +120 mGals at the shelf break and a rather broad low of -30 to -60 mGals over the continental rise. A low of -30 to -90 mGals occurs over the inner shelf in that part of the

margin associated with the offshore sedimentary basins. Specifically, the Barreirinhas/Piaui-Camocim basin is associated with a minimum Bouguer gravity value of -60 to -90 mGals along the depocenter onshore and a minimum Free-air gravity value of -30 to -60 mGals offshore. Much higher gravity values in the range of +30 to +60 mGals occur along the continental shelf eastward of this basin. The typical free-air gravity anomaly "edge effect" is absent along the eastern portion of the continental margin bounded by the Romanche and Fernando de Noronha Fracture Zones. Isolated highs occur on the continental shelf in this area related to local structural highs such as the Fortaleza and Touros High.

The maximum gravity value within the study area is slightly above 180 mGals and occurs at the Ceara guyot. The gravity expression of the Romanche and Fernando de Noronha fracture zones correspond to well-defined lineations trending EW with maximum and minimum values of +90 to +120 mGals and -30 to -60 mGals respectively.

5 - ISOSTASY AND PLATE DEFORMATION

The condition of isostasy or total compensation relies on the assumption that, at a depth (d_C) beneath the surface, the lithostatic stresses are equal. This hydrostatic equilibrium concept can be expressed in terms of the density distribution in the lithosphere as follows (Dehlinger, 1978; Turcotte, 1979; Turcotte and Schubbert, 1982) :

$$\int_0^{d_c} \Delta\rho(z)\, dz = 0 \qquad (1)$$

An elementary application of the principle of isostasy is the subsidence of passive continental margins due to sediment load. This study focuses on two simple isostatic models : Airy and plate flexure. In the Airy model the crust cannot support any vertical shear stresses, whereas, in the plate model, also known as the Vening Meinesz regional isostatic model, the lithosphere flexes allowing for lateral stress differences (figure 8). The concentrated load is, therefore, supported over an area considerably larger than itself by the buoyancy forces on the base of the plate (Banks et al, 1977) . Since the Airy model or local compensation model can be envisioned as an end member of the plate model, for a lithosphere for which the mechanical strength is null, I use a generalized approach that treats the lithosphere as a thin elastic plate (plate thickness is small in comparison tothe wavelength of the deformation).

Assuming that the outer shell of the Earth behaves like a thin, continuous and homogeneous elastic plate floating in an inviscid fluid, the governing equation for the vertical deformation w(**r**) due to a load p(**r**) is (Jeffreys, 1976 ; Banks et al., 1977; Turcotte, 1979) :

$$D\, \nabla^4 w(\mathbf{r}) = p(\mathbf{r}) \qquad (2)$$

where :

r - position vector $\mathbf{r} = (x,y,z)$

D - flexural rigidity ; this parameter is as a measure of the flexural strength of the lithosphere, the resistance of a plate to bending; strictly speaking, D refers to the apparent flexural rigidity since the horizontal forces acting on the plane are neglected in expression (2); if the plate is continuous, homogeneous and elastic, D is related to the Young's modulus (E) of the plate , its elastic thickness (T_e) and Poisson's ratio (υ) as follows :

$$D = \frac{E T_e^3}{12 (1 - \upsilon^2)} \qquad (3a)$$

w(**r**) - plate deflection measured positively downwards; strictly speaking it is the deformation of the median plane within the plate caused by a topographic load $h_o(\mathbf{r})$; however for thin elastic plates it is valid to assume that the top and bottom surfaces deform similarly (Banks et al, 1977; Turcotte and Schubbert, 1982). The half-width of the load $h_o(\mathbf{r})$ is related to the flexural parameter and, therefore, to the flexural rigidity of the plate as follows (figure 3):

$$\text{Half width} = \frac{\pi}{4} \alpha_F \qquad (3b)$$

$$\alpha_F = \left[\frac{4 D}{(\rho_m - \rho_0) g} \right]^{1/4} \qquad (3c)$$

p(**r**) - net upward force acting on the plate per unit area.It is caused by the topographic load $h_o(\mathbf{r})$ of density ρ_o and the buoyancy force due to the displacement of the asthenosphere ρ_m by the flexing lithospheric plate (figure 8).

$$p(\mathbf{r}) = - \rho_o g h_o(\mathbf{r}) - \rho_m g w(\mathbf{r}) \qquad (4)$$

The observed topography h(**r**) can be expressed as the result of the load topography h_o(**r**) and the plate deformation w(**r**) (Banks et al., 1977) :

$$h(\mathbf{r}) = h_o(\mathbf{r}) + w(\mathbf{r}) \tag{5}$$

Substituting expression (4) in (2) and taking the two-dimensional fourier transform yields :

$$\mathbf{k}^4 D\, W(\mathbf{k}) = -\rho_o g\, H_o(\mathbf{k}) - \rho_m g\, W(\mathbf{k}) \tag{6}$$

where :

$$W(\mathbf{k}) = \frac{1}{2\pi} \int_s w(\mathbf{r}) \exp(i\mathbf{kr})\, ds$$

$$H_o(\mathbf{k}) = \frac{1}{2\pi} \int_s h_o(\mathbf{r}) \exp(i\mathbf{kr})\, ds$$

The expression that relates plate deformation to topography as a function of the mechanical properties of the plate is obtained by replacing H_o(**r**) by H(**r**) and W(**r**) according to expression (5) (Banks et. al., 1977) :

$$W(k) = \frac{\rho_o}{\rho_m - \rho_o} \left[1 + \frac{k^4 D}{(\rho_m - \rho_o) g} \right]^{-1} H(k) \tag{7}$$

where :

g - gravitational constant

The application of the analytic solution presented above for the plate deformation will become obvious in the formulation of the theoretical admittance expressions (section 6.2) .

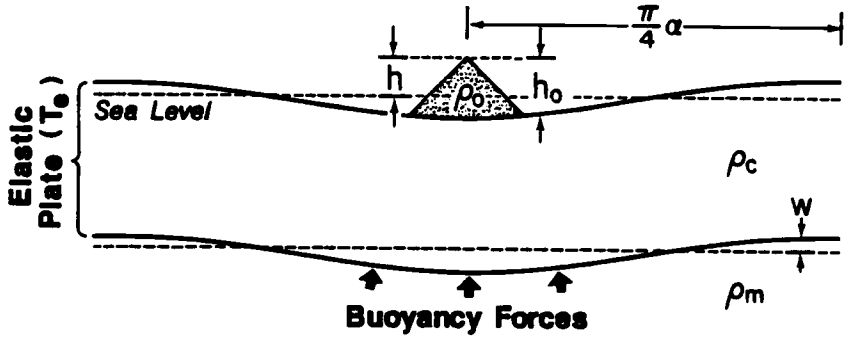

Figure 8 - Schematic representation of a continuous elastic plate loaded at the top.

6 - ADMITTANCE ANALYSIS

6.1 - THEORETICAL AND PRACTICAL CONSIDERATIONS

Assuming that the earth is linear and isotropic in its response to a delta function load, Dorman and Lewis (1970) have shown that the gravity field $g_b(\mathbf{r})$ can be expressed as a two-dimensional convolution of the unknown isostatic response function $q(\mathbf{r})$ with the topography $h(\mathbf{r})$ plus a term n related to lateral density variations in the crust and/or upper mantle :

$$g_b(\mathbf{r}) = \int_s q\,|\,\mathbf{r}_o - \mathbf{r}\,|\,h(\mathbf{r})\,ds + n \qquad (8)$$

$$= q * h + n$$

The second term in expression (8) , which relates that part of the Bouguer anomaly not caused by isostatic compensation, can be neglected as it it is uncorrelated with q*h (Dorman and Lewis, 1970; McNutt, 1982) . Since the convolution operation becomes a simple multiplication in the Fourier domain the isostatic response function can be easily obtained from the inverse transform of the ratio of the transforms of the Bouguer gravity field to topography.

$$G(\mathbf{k})=Q(\mathbf{k})\,H(\mathbf{k}) \qquad (9)$$

where :

$$\mathbf{k}_n = \sqrt{k_x + k_y} = n\,\frac{2\pi}{L} \qquad n = 0,1,2 \ldots L/2\Delta x$$

L - length of the spatial data series

Δx - sampling interval

By analogy, for oceanic areas, the free-air response function Z(k), also called gravitational admittance or linear transfer function, replaces the isostatic response function Q(k).

$$G(\mathbf{k}) = Z(\mathbf{k})\, B(\mathbf{k}) \qquad (10)$$

where:

$B(\mathbf{k})$ - discrete Fourier transform of the bathymetry data series

In this study, I assume that gravity and bathymetry are one - dimensional, that is, always perpendicular to the ship track so that $|\mathbf{k}|$ is then related to k, the wavenumber along track. The use of k instead of $|\mathbf{k}|$ is considered to be a good approximation since features along the margin trend EW and the tracklines trend NS. Ribe (1982) discusses the implications of the 1-dimensionality assumption when the geological features are not linear, e.g. , seamounts.

According to expression (9) the experimental complex admittance can be obtained from observational data by dividing the Fourier transforms of gravity by bathymetry over a given tectonic province. However, due to the presence of noise, the admittance estimates are unstable and biased as shown by Munk and Cartwright (1966) in transfer function studies of tidal heights. The method commonly used to obtain the complex admittance function follows Watts' (1978) approach. It consists of obtaining independent estimates of the cross spectrum of bathymetry and gravity for each data series, averaging the results over N profiles within a given tectonic province and then using the resulting smoothed

spectra to obtain admittance. The averaged cross spectrum and power spectra of g(x) and b(x), $< C (k_n) >$, $< E_g (k_n) >$ and $< E_b (k_n) >$ respectively, are given by :

$$< C (k_n) > = \frac{1}{N} \sum_{r=1}^{N} G_r (k_n) B_r^* (k_n) \tag{11}$$

$$< E_G (k_n) > = \frac{1}{N} \sum_{r=1}^{N} G_r (k_n) G_r^* (k_n) \tag{12}$$

$$< E_B (k_n) > = \frac{1}{N} \sum_{r=1}^{N} B_r (k_n) B_r^* (k_n) \tag{13}$$

where :

$k_n = n \frac{2\pi}{L}$ $\qquad n = 0,1,2 \ldots L/2\Delta x$

$G (k_n)$, $B (k_n)$ - discrete fast Fourier transform of g(x) and b(x).

G^*, B^* - complex conjugate of G, B

N - number of profiles.

The best estimate, in a least squares sense, of the experimental complex admittance is given by :

$$Z(k_n) = \frac{<C(k_n)>}{<E_B(k_n)>} \tag{14}$$

The uncertainties in the experimental admittance estimates are commonly expressed in terms of two estimates : coherence γ^2 , which represents a measure of that fraction of the gravity which can be predicted from bathymetry at a particular spatial frequency and the

phase $\phi(k_n)$ which should be close to zero if no offset exists between a given bathymetric feature and its gravity expression.

$$\gamma^2 = \frac{C(k_n)\, C^*(k_n)}{E_B(k_n)\, E_G(k_n)} \tag{15}$$

$$\phi(k_n) = \tan^{-1}\left(\frac{Im(Z(k_n))}{Re(Z(k_n))}\right) \tag{16}$$

However, Munk and Cartwright (1966) have shown that the coherence estimates obtained, as described above, are biased by noise in the gravity data and have suggested using :

$$\gamma^2(k_n) = \frac{\left[\, N \left(\frac{C(k_n)\, C^*(k_n)}{E_B(k_n)\, E_G(k_n)}\right) - 1 \,\right]}{N-1} \tag{17}$$

Assuming that the noise present in the observational series is normally distributed with zero mean, the unbiased variance of Z(kn), dependant upon the coherence, is given by (Ribe,1982):

$$\sigma^2 = \frac{\gamma^{-2} - 1}{2(N-1)} \, |Z(k_n)|^2 \tag{18}$$

6.2 - LINEAR ISOSTATIC MODELS IN THE FOURIER DOMAIN

Parker (1972) has shown that the Fourier domain gravity effect of a given uneven and non-uniform topographic surface h(x) of density ρ at a depth d from the measuring plane can be expressed as an infinite series of Fourier transforms:

$$G(\mathbf{k}_n) = 2\pi\rho\gamma \exp(-|\mathbf{k}_n| d) \sum_{n=1}^{\infty} \frac{|\mathbf{k}_n|^{n-1}}{n!} H^n(\mathbf{k}_n) \qquad (19)$$

where :

γ - gravitational constant.

$H(\mathbf{k}_n)$ - discrete Fourier transform of h(x).

d - mean elevation ($d >> h(x)$)

Neglecting the higher order terms and assuming a 1-D analysis it follows that :

$$G(k_n) = 2\pi\rho\gamma \exp(-|k_n| d) H(k_n) \qquad (20)$$

The gravity effect of the surface topography $G_1(k_n)$ and its corresponding root $G_2(k_n)$ can be expressed as :

$$G_1(k_n) = 2\pi \Delta\rho_1 \gamma \exp(-|k_n| d) H(k_n) \qquad (21)$$

$$G_2(k_n) = -2\pi \Delta\rho_2 \gamma \exp[-|k_n| (d + T_{ca})] R(k_n) \qquad (22)$$

where :

$R(k_n)$ - discrete fourier transform of the root topography $\rho(x)$.

$\Delta\rho_1$ - density contrast across the topography h(x); in this study it refers to the density contrast between the sediments (ρ_s) and sea water (ρ_w).

$\Delta\rho_2$ - density contrast across the root topography $\rho(x)$; in this study it refers to the density contrast between the mantle (ρ_m) and crust (ρ_c).

T_{ca} - distance between the mean root surface and mean topography as shown in figure 9 (also called the apparent crustal thickness). For simplicity it is assumed that compensation occurs at depth T_c. According to Karner and Watts (1982), the relation between the crustal thickness at the coastline T_c and the apparent crustal thickness T_{ca} is:

$$T_{ca} = T_c - (d/2) \left[(\rho_m - \rho_w) / (\rho_m - \rho_s) \right]$$

For a two-layer model, the gravity anomaly at a given geological feature $G_t(k_n)$ is simply the sum of the gravity effect of each layer, that is :

$$G_T(k_n) = G_1(k_n) + G_2(k_n)$$

$$G_T(k_n) = 2\pi\Delta\rho_1 \gamma \exp(-|k_n| d)\left(1 - \frac{\Delta\rho_2}{\Delta\rho_1}\left[\frac{R(k_n)}{H(k_n)}\right]\exp(-|k_n| T_{ca})\right)H(k_n) \qquad (23)$$

Assuming that the lithosphere behaves like a thin homogeneous elastic plate, the expression derived for the plate deformation W(k) in section 6.1 (expression 7) can be used to express the root topography R(k) in the Fourier domain (Banks et al., 1977):

$$R(k_n) = \frac{\Delta\rho_1}{\Delta\rho_3}\left[1 + \frac{k_n^4 D}{\Delta\rho_3 g}\right]^{-1} H(k_n) \qquad (24)$$

where :

$\Delta\rho_3$ - density contrast between the material overlying and underlying the elastic plate, ($= \rho_m - \rho_s$)

Substituting expression (24) into (23) and normalizing by H(k) we obtain a general theoretical expression for the plate admittance Z(k) on margins (Karner and Watts, 1982).

$$Z(k_n)= 2\pi\gamma(\rho_s-\rho_w)\exp(-k_n d)\left\{1-\frac{(\rho_m-\rho_f)}{(\rho_m-\rho_s)}\left[1+\frac{(k_n)^4 D}{(\rho_m-\rho_s)g}\right]^{-1}\exp(-k_n T_{ca})\right\} \qquad (25)$$

The Airy admittance represents a special case of the expression above by letting $D\rightarrow 0$ and $\Delta\rho_3 \rightarrow \Delta\rho_2$.

$$Z(k_n) = 2\pi\gamma(\rho_s-\rho_w)\exp(-k_n d)(1-\exp(-k_n T_{ca})) \qquad (26)$$

The normalization of expression (20) by H(k) yields the admittance expression for uncompensated topography :

$$Z(k_n) = 2\pi\gamma(\rho_s-\rho_w)\exp(-k_n d) \qquad (27)$$

The expression above gives a straight line when ln | Z (k) | is plotted against wavenumber. The mean water depth (d) and topography density (ρ_2) can be estimated from the negative slope and intercept ln ($2\pi\gamma(\rho_s-\rho_w)$ respectively.

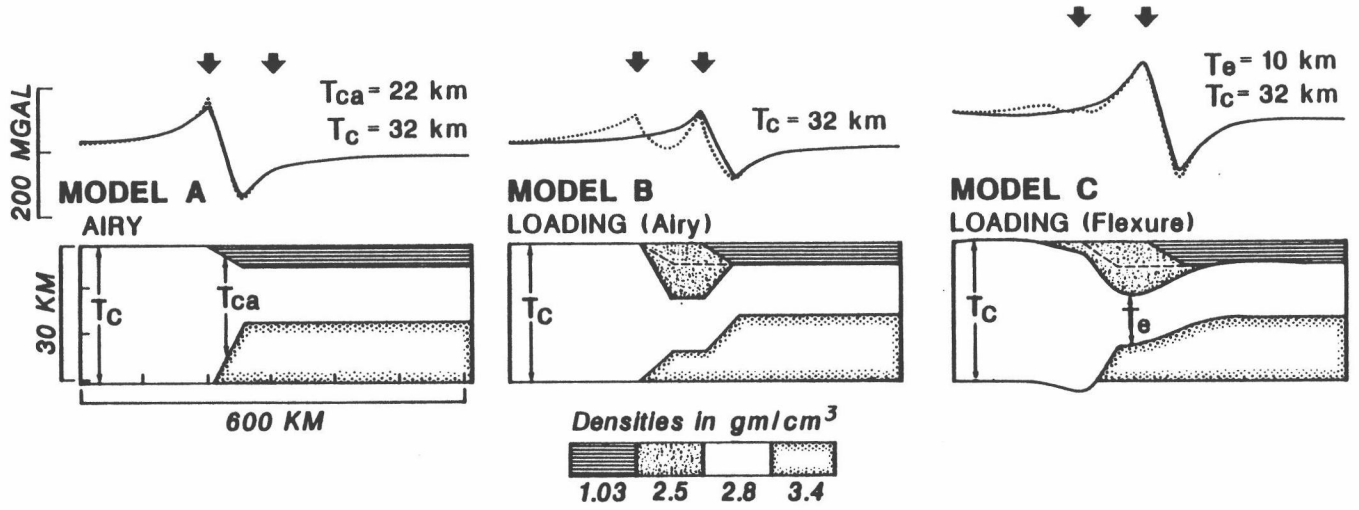

Figure 9 - Scheme showing the theoretical crustal structure of a passive margin under different compensating mechanisms. Model A shows a "starved" margin (only water loading) and the corresponding gravity effect obtained by the line integral method (dotted lines) and the Fourier method (solid lines). Errors introduced by neglecting the high order terms (expression 20) are resposible for the small departures seen at the inflection points. Sediment loading of a passive margin with no flexural rigidity ($T_e = 0$) shown in model B (Airy loading) is characterized by a double-peaked gravity anomaly. Because only the shelf break has bathymetric expression, the gravity effect calculated using the Fourier method cannot reproduce the peak along the hinge line . Model C shows sediments loading a margin when $T_e > 0$ (Flexural loading). Note that as T_e increases from zero (model B) to 10 km (model C) the energy in the gravity anomaly, initially divided into the hinge line and shelf break, is transferred to the shelf break. T_c refers to the crustal thickness at the coastline, where unstretched or sligthly stretched continental crust is believed to occur, and T_{ca} refers to the apparent crustal thickness (from Karner and Watts, 1982).

6.3 - DATA TREATMENT APPROACH - MINIMIZING TRUNCATION EFFECTS

As mentioned in the discussion above, in order to calculate the experimental admittance function, we need to obtain the discrete FFT estimates of the free-air gravity and bathymetry data series. For this purpose, we assume that both series are periodic, with periods ΔxN. Since this is not the case, abrupt discontinuities introduced by the rectangular window can occur if the ends of each profile are not smoothed or tapered, leading to aliasing.

The sharp steps in the space domain introduced by the rectangular window can be reduced by removing the mean of each profile. In addition to the removal of the mean, McKenzie and Bowin (1976) and Louden (1981) have also subtracted the first order trend from each of the profiles . However, if both ends of the data series do not merge smoothly, artificial high frequencies might still be present. Furthermore, for some tectonic provinces such as fracture zones (Louden and Forsyth, 1982) and continental margins (Karner and Watts,1982), the first order trend has an inherent geodynamical meaning. For instance, lithospheric plates of different thermal ages, such as across a fracture zone, require a thicker crust on the older side creating a long-wavelength edge-effect anomaly. The removal of this regional trend will obviously affect the the long-wavelength admittance estimates. The same occurs along passive margins where the shallowing of the mantle past the hinge line, also creates a long-wavelength anomaly. Instead of removing the first order trend, the same authors have chosen to convert each data series into an even function about the origin by reflecting the profiles, yielding real transforms . Louden and Forsyth (1982) also suggested that the even and odd wavenumbers can be analysed separately and, therefore, the edge effect, which is anti-symmetric about the trough of the fracture zone,

can be isolated. This "artifact" enabled them to analyse the possible compensating mechanisms for the surface topography without interference of the edge effect .

Another common data treatment procedure consists of applying tapers at the ends of the data series (Watts,1978; Ribe and Watts, 1982; McNutt (1983); Young and Hill, 1986). However, McNutt (1983) has shown that the use of a Gaussian or cosine taper for two-dimensional arrays leads to an overestimation of the experimental admittance function at mid-wavelengths. This is due to the fact that the tapering method increases the G(k)/B(k) ratio which forces a perfect correlation between gravity and bathymetry corresponding to the width of the taper. More recently, Diament (1985) has suggested, for the first time, the use of the first derivatives of the profiles.

Because of the controversy regarding the best technique of minimizing the truncation effect caused by the infinite length series assumption in the FFT algorithm, I decided to carry out several tests on the gravity and bathymetry data available for the equatorial margin of Brazil. The approach I adopted is similar to the one used by McNutt (1983) on a 2-D topography array and consists of testing how reliably a given admittance estimate can be recovered as a function of the data treatment procedure. Figure 10 shows the four different procedures used to minimize truncation effects: removal of the first order trend (T_1), cosine tapering applied to 10% of the total length (T_2), reflecting the profiles (mirror imaging) (T_3) and the use of an approximation to the first derivatives (T_4). These were obtained using Newton's divided-difference interpolating polynomial approach. The approximation to the first derivative ($f[x,x_o]$), termed the first finite divided difference or finite divided difference of order one, is given by :

$$f[x,x_o] = \frac{f(x) - f(x_o)}{x - x_o}$$

where :

f(xo), f(x) - data (gravity and bathymetry) at position xo,x

xo,x - horizontal position; the data are equispaced

Twelve profiles, each 256 km long, were extracted from gridded gravity and bathymetry (figure 10). Profiles 4, 5 and 6 were specifically used for testing the different data treatment procedures. They have been linearly interpolated to a sampling interval of 1 km and the mean removed before employing each procedure to avoid aliasing (except for case d). A "predicted" gravity profile $g_p(x)$ is then generated by convolving each bathymetric profile b(x) with a theoretical admittance filter z(x):

$$g_p(x) = z(x) * b(x) \tag{28}$$

Assuming local compensation, the theoretical admittance filter was obtained by the inverse transform of expression (26) :

$$z(x) = \gamma (\rho_s - \rho_w) \left[\frac{d/\pi}{d^2 + x^2} - \frac{d + T/\pi}{(d + T_{ca})^2 + x^2} \right] \tag{29}$$

where :

x - horizontal distance

In the computation of the filter shown in figure 13 an apparent crustal thickness of 18 km at the coastline and sediment density of 2.2 g/cm3 were used. The ends of the "predicted" gravity signal are then subjected to the same treatment as the corresponding bathymetric profile before Fourier transforming both profiles. The experimental admittance estimates are then calculated using expression (14). Figure 14 shows the admittance estimates obtained using the bathymetry and "predicted" gravity profiles for the four different data treatment procedures. Among the different data treatments, tested in this study, the use of the first derivative appears to be the most appropriate. This confirms

Diament's (1985) results, although he used a different approach and did not consider mirror imaging in his final analysis. The mirror imaging technique produces slightly better admittance estimates than applying the 10% cosine taper. In order to investigate the stability of the long-wavelength admittance estimates in the presence of noise, I conducted several tests using a noisy "predicted" gravity obtained by introducing Gaussian noise in the range of -50 to +50 mGals. Figure 15 shows the results of this analysis. Once again, the use of the first derivatives yields the most reliable admittance estimates. In the presence of noise, the mirroring technique yields admittance estimates more reliable than the tapering methods, although, the admittance values are overestimated.

It is important to point out that although the mirror imaging procedure has been used in the previous admittance studies on continental margins (Karner and Watts, 1982; Mello and Bender, 1988), there is no interpretational advantage related to this data treatment. This is not the case for fracture zone studies in which the even and odd wavenumbers can be analysed separately in order to isolate the part of the signal exclusively related to the edge effect (Louden and Forsyth, 1982). Since the gravity and bathymetry signatures are not symmetric about the shelf edge, this "artifact " cannot be used. Furthermore, because mirror imaging forces the real data series to be even functions, it invalidates the phase analysis since the corresponding Fourier transform will have zero phase . Therefore, considering the items above and the results shown in figures 14 and 15, I decided to use the first derivatives of the observational data series in this study.

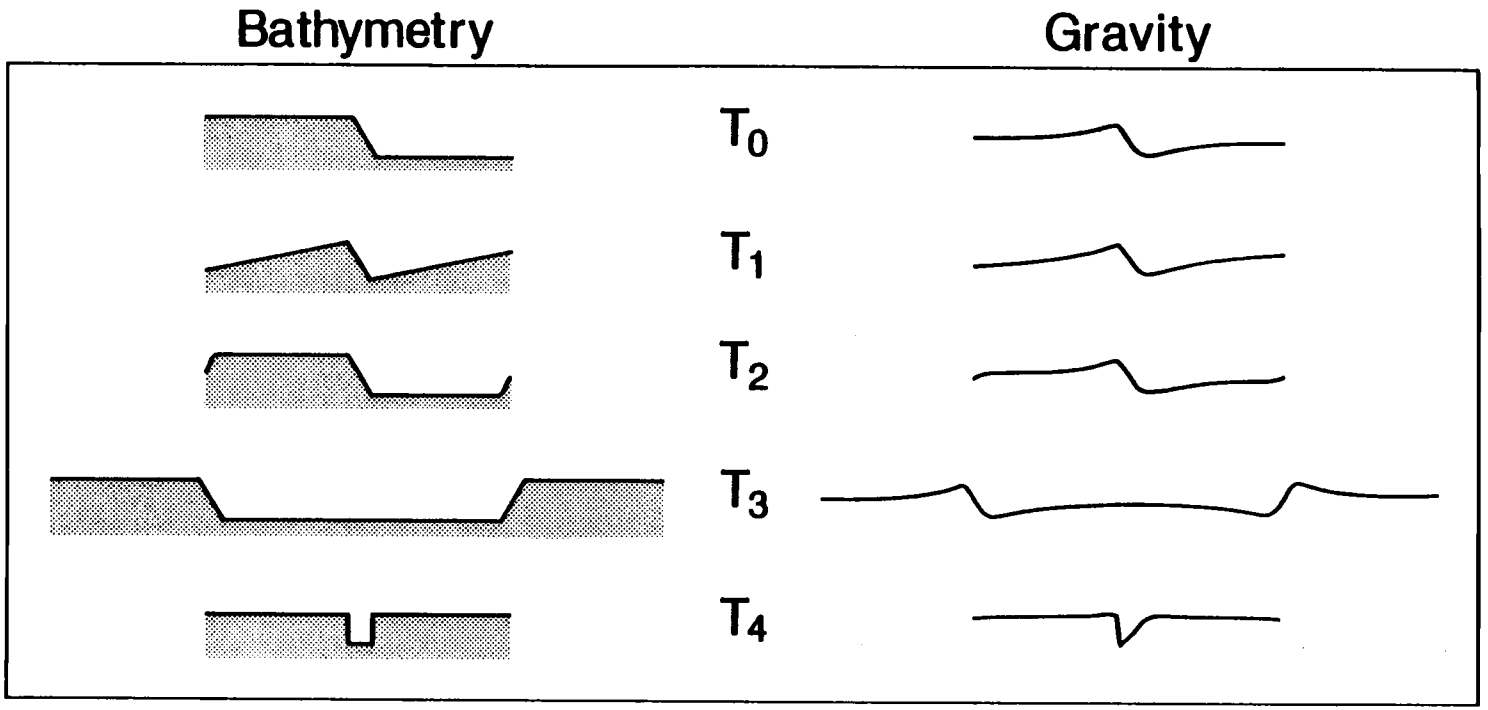

Figure 10 - T_0 shows a synthetic gravity and bathymetric profile along a passive margin. The different data treatment procedures are illustrated: removal of the trend (T_1), cosine tapering (T_2), mirror imaging (T_3) and the use of the first derivatives (T_4). The mean of the synthetic profiles were removed before applying each procedure (except for T_4)

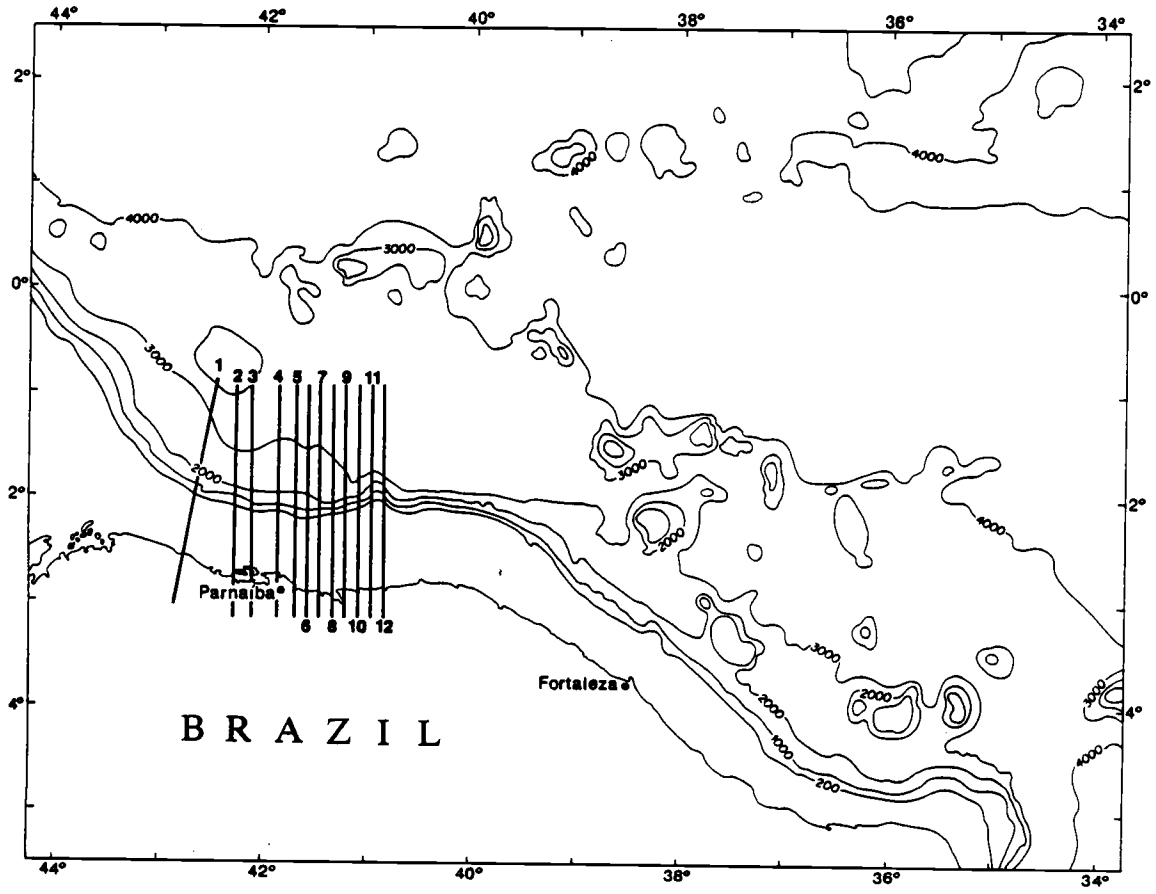

Figure 11 - Location of the gravity and bathymetry profiles (1-12) used in the admittance analysis. Isobaths are in meters.

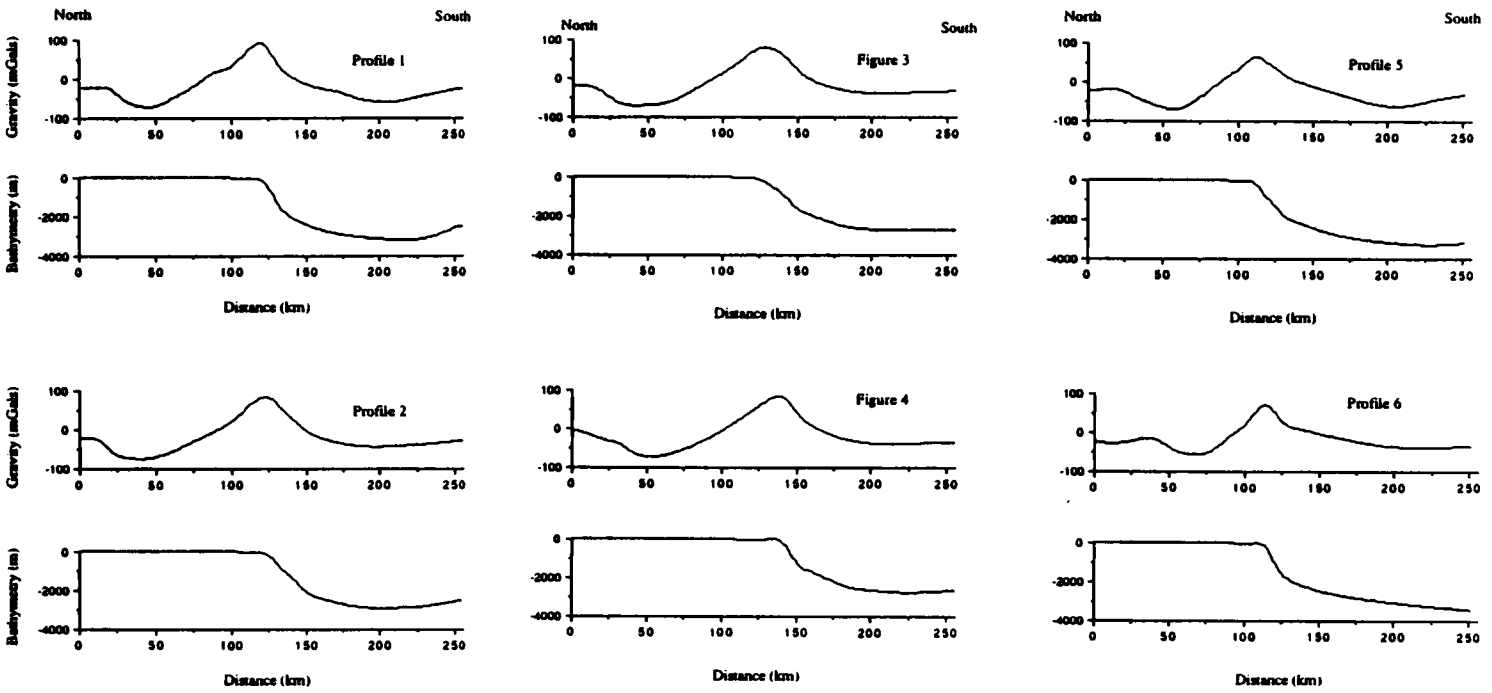

Figure 12 - Twelve gravity and bathymetry profiles used in the admittance analysis

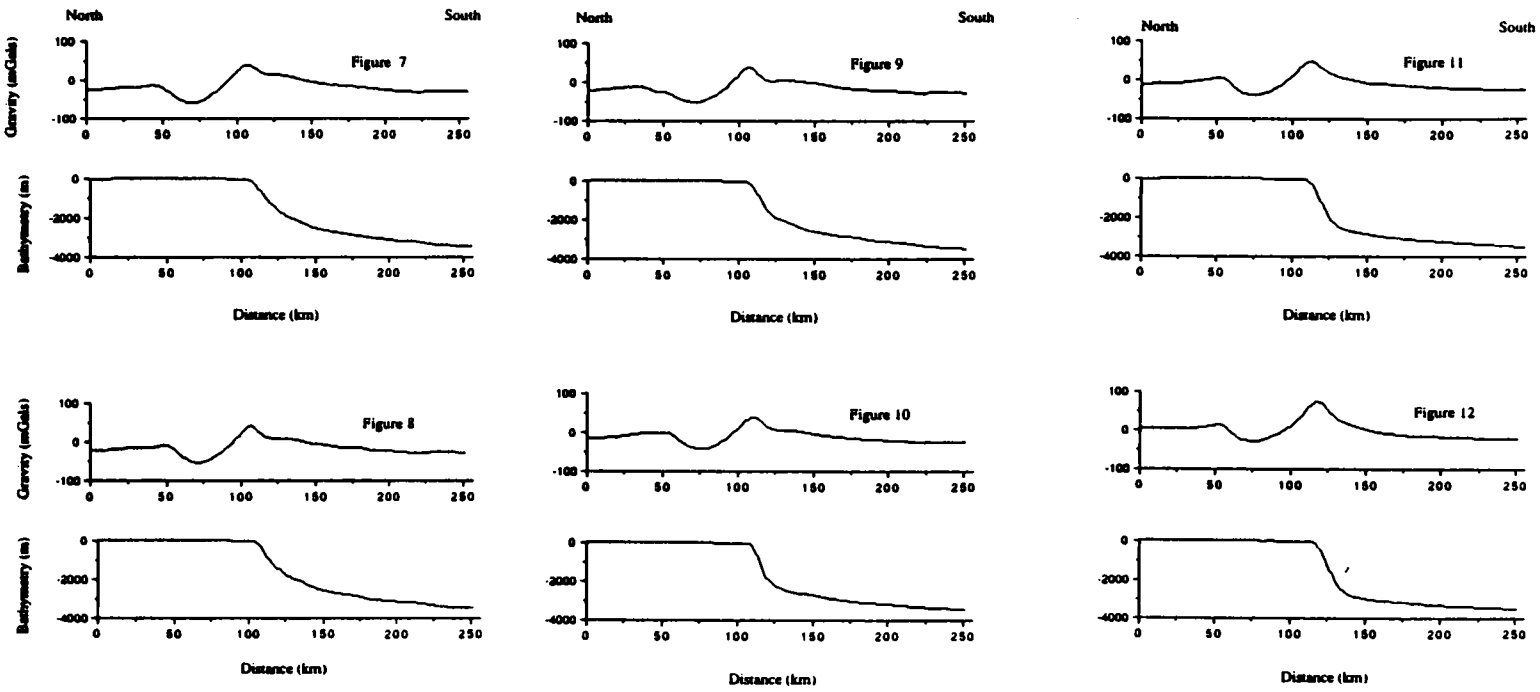

Figure 12 - Continued

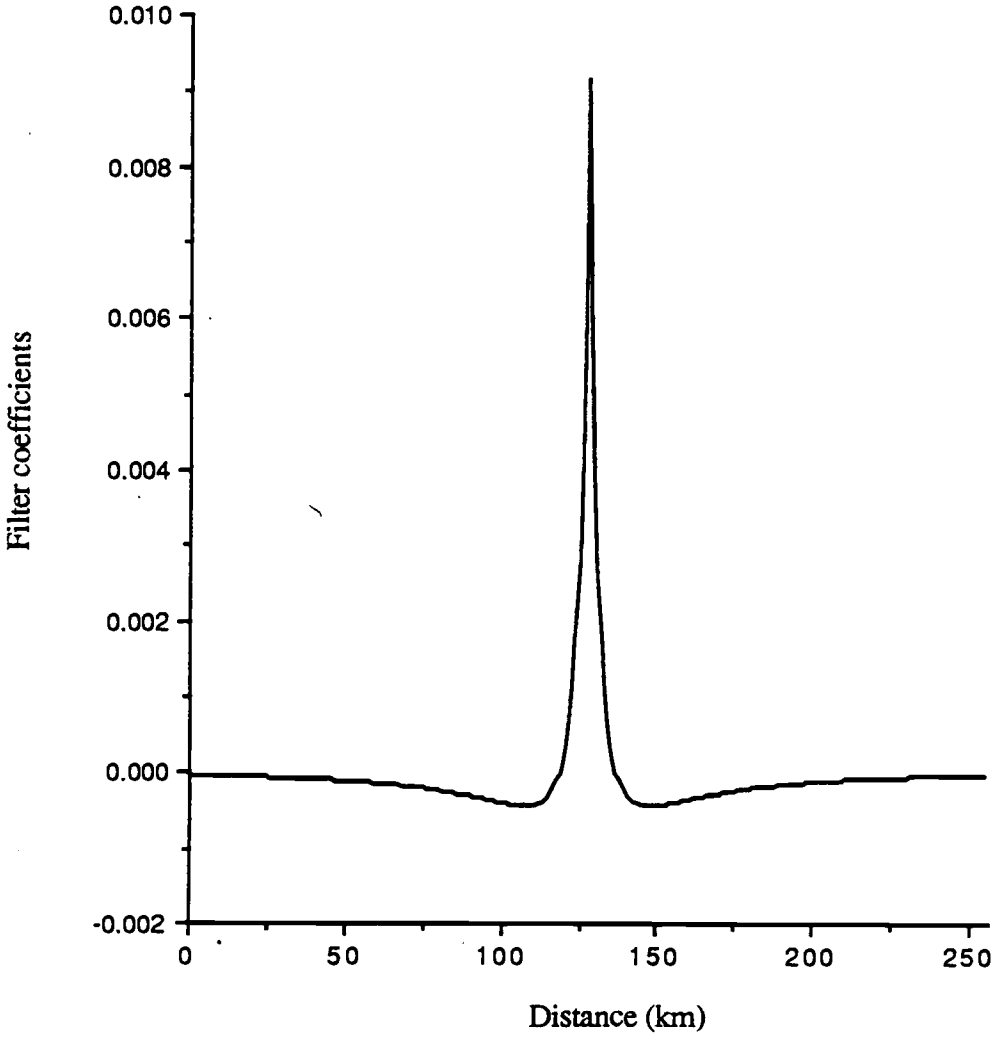

Figure 13 - Admittance filter used to generate the "predicted" gravity. Space domain representation of the admittance function for the Airy model, with apparent crustal thickness of 18 km, and sediment density of 2.2 g/cc.

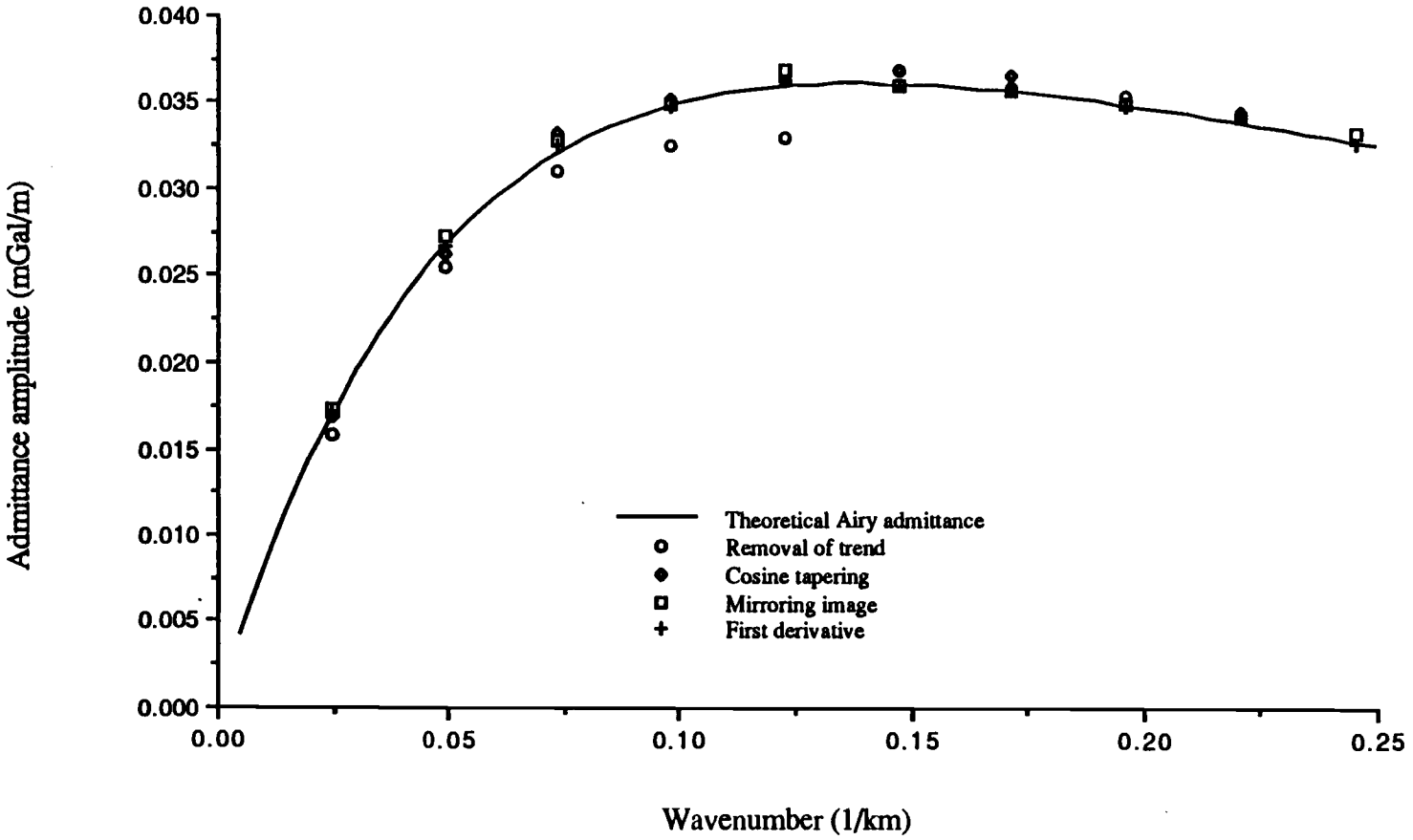

Figure 14 - Theoretical admittance function for the Airy model (solid line) and experimental admittance estimates obtained using the "predicted" gravity for 4 different data treatment procedures

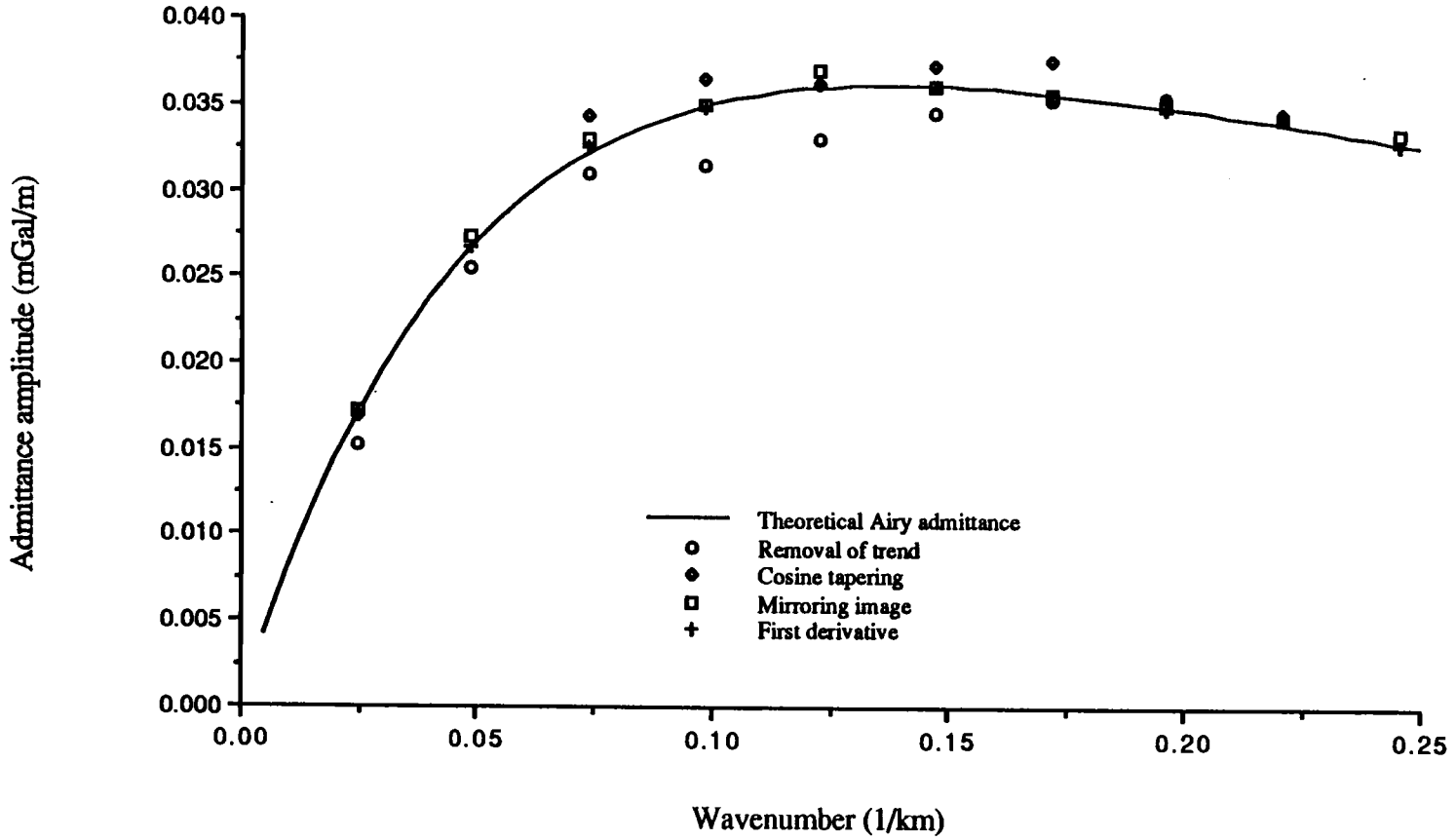

Figure 15 - Theoretical admittance function for the Airy model (solid line) and experimental admittance estimates obtained using the "predicted" gravity with random noise.

6.4 - EXPERIMENTAL ADMITTANCE VS. THEORETICAL ADMITTANCE

As shown in section 6.2, the experimental admittance estimates are obtained directly from observational data and, therefore, are not tied to any *a priori* isostatic compensating mechanism. This offers the particular advantage of being able to interpret the admittance estimates in terms of linearized regional and local isostatic models (expressions 25 and 26), from which information on the long-term mechanical strength of the lithosphere may be obtained.

Figure 16 shows a plot of the amplitude for a given admittance function against wavenumber. The waveband $0.025\ km^{-1} < k < 0.08\ km^{-1}$ ($250\ km > l > 80\ km$) is called the diagnostic waveband, since it comprises the wavenumbers for which the coherence estimates are expected to be high ($\sigma^2 > 0.75$), and displays significant changes as a function of T_{ca} (apparent crustal thickness) or T_e (apparent or effective elastic thickness). The admittance function can be pictured as a filter that attenuates the bathymetry spectrum at low and high wavenumbers, allowing the signal in the intermediate wavenumber band to pass. The width of this "intermediate-pass" filter is a function of the mechanical strength of the lithosphere. As far as the short-wavelengths are concerned, many authors have used the uncompensated waveband ($k > 0.14\ km^{-1}$) to obtain estimates for the the density contrast across the topography ($\rho_w - \rho_s$) and mean water depth as demonstrated above (expression 27). However, Ribe (1982) pointed out several reasons for not pursuing this approach, particularly when the observational data series have been linearly interpolated.

As mentioned before, 12 profiles, each 256 km long, oriented perpendicular to the major EW structural trend were taken from gridded gravity and bathymetry data (figure 12). Each gravity and bathymetric series was linearly interpolated using a sampling interval

of 1 km. The first derivative of each profile was then Fourier transformed. Independent estimates of the cross spectra and power spectra of the derivatives of the bathymetry and gravity series were obtained and averaged over the 12 profiles (expressions 11, 12 and 13). The smoothed spectra were used to obtain the experimental admittance estimates (expression 14). The amplitude of the experimental admittance, as a function of the wavenumber and the corresponding filter in the space domain, are shown in figures 17 and 18 respectively. The amplitude of the admittance decreases for wavelengths less than 50 km, showing the filtering effect of the water layer. Figures 19 and 20 show the coherence and phase plots for the experimental admittance function. As stated earlier, the coherence represents a measure of the fraction of the gravity field which can be predicted by a linear filter acting on the bathymetry. At long wavelengths, gravity and bathymetry are correlated and, therefore, the coherence approaches one. On the other hand, at short wavelengths gravity and bathymetry are uncorrelated and, therefore, coherence is close to zero. Although the coherence values in the diagnostic waveband are consistently greater than 0.75, large phase oscillations between +80 and -80 degrees were observed. This large phase offset is associated with the Barreirinhas/Piaui-Camocin basin since it does not have any topographic/bathymertric expression.

Figures 21(a) and 21(b) show the experimental admittance estimates as a function of the wavenumber. The solid curves in figure 21(a) represent the theoretical Airy (T_e=0) admittance for a range of values for the apparent crustal thickness (T_{ca}), whereas, in figure 21(b) they represent the theoretical admittance for the plate flexure model for varying effective elastic thickness ($T_e \neq 0$). An apparent crustal thickness of 18 km was used to construct the theoretical curves for the plate model . The experimental admittance estimates show significant departures from the theoretical curves for both isostatic models, in terms of amplitude and overall shape. The peak in the admittance estimates occur at k = 0.10

km^{-1} showing about a 63 km shift in comparison to the expected "broad" and much lower amplitude (at least a 0.025 mGals/m difference) displayed in the theoretical curves.

Table I provides a list of the input parameters used in the calculation of the theoretical curves. The value for the sediment density used in the preparation of the simple Bouguer maps along the shelf is based on Petrobras internal reports and represents an average for the sedimentary sequence. The mean water depth was obtained from the average of the 12 profiles.

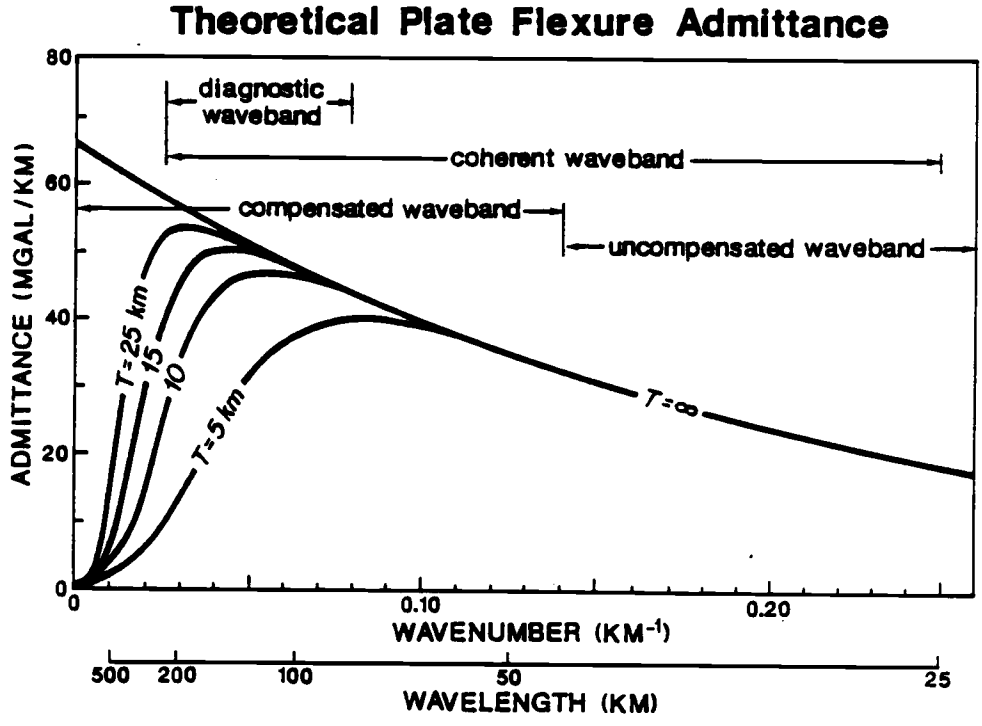

Figure 16 - Theoretical admittance for the plate flexure model for varying values of effective elastic thickness T_e (expression 25). Information on the mechanical strength of the lithosphere (T_e values) may be obtained from the experimental admittance estimates in the diagnostic waveband. The admittance for uncompensated topography corresponds to $T_e \rightarrow \infty$ (expression 27). The coherent waveband denotes the wavenumber band for which coherence > 0.75 (from Watts et al., 1980).

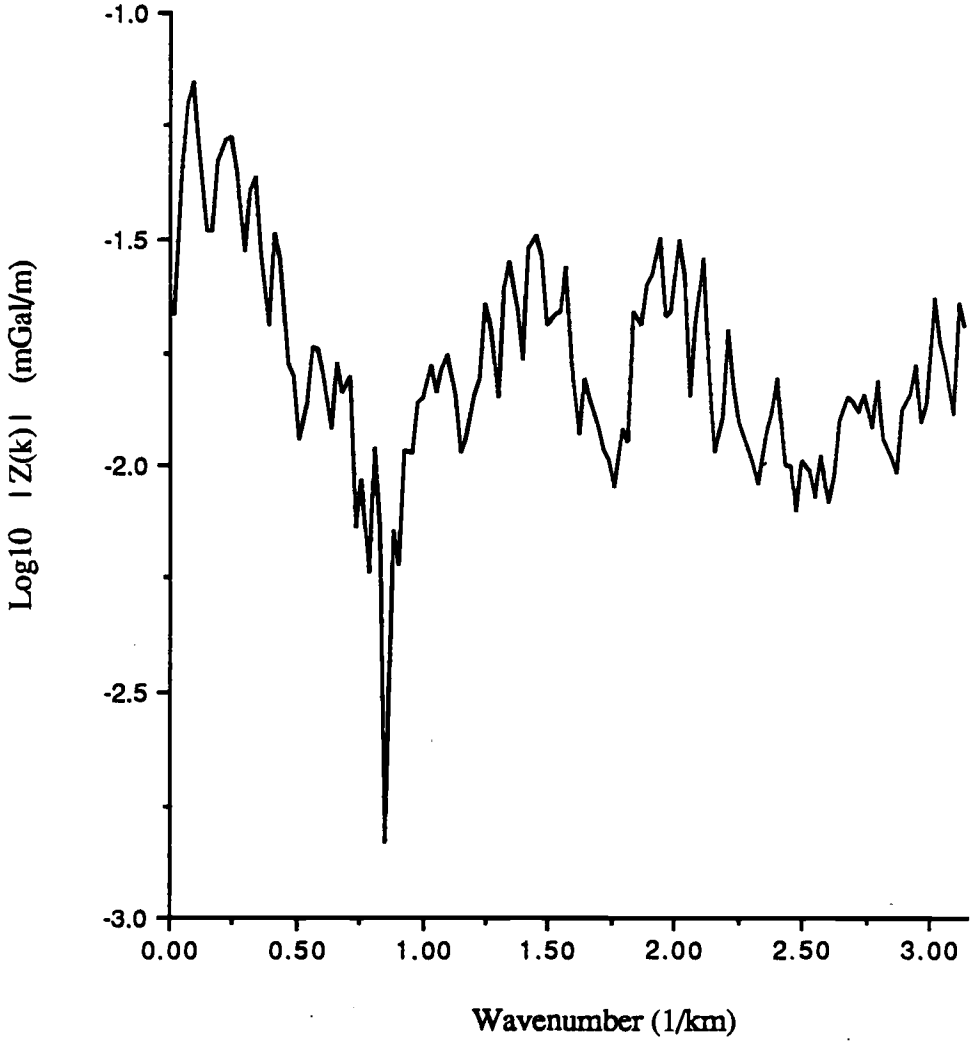

Figure 17 - Log10 of the experimental admittance plotted against wavenumber

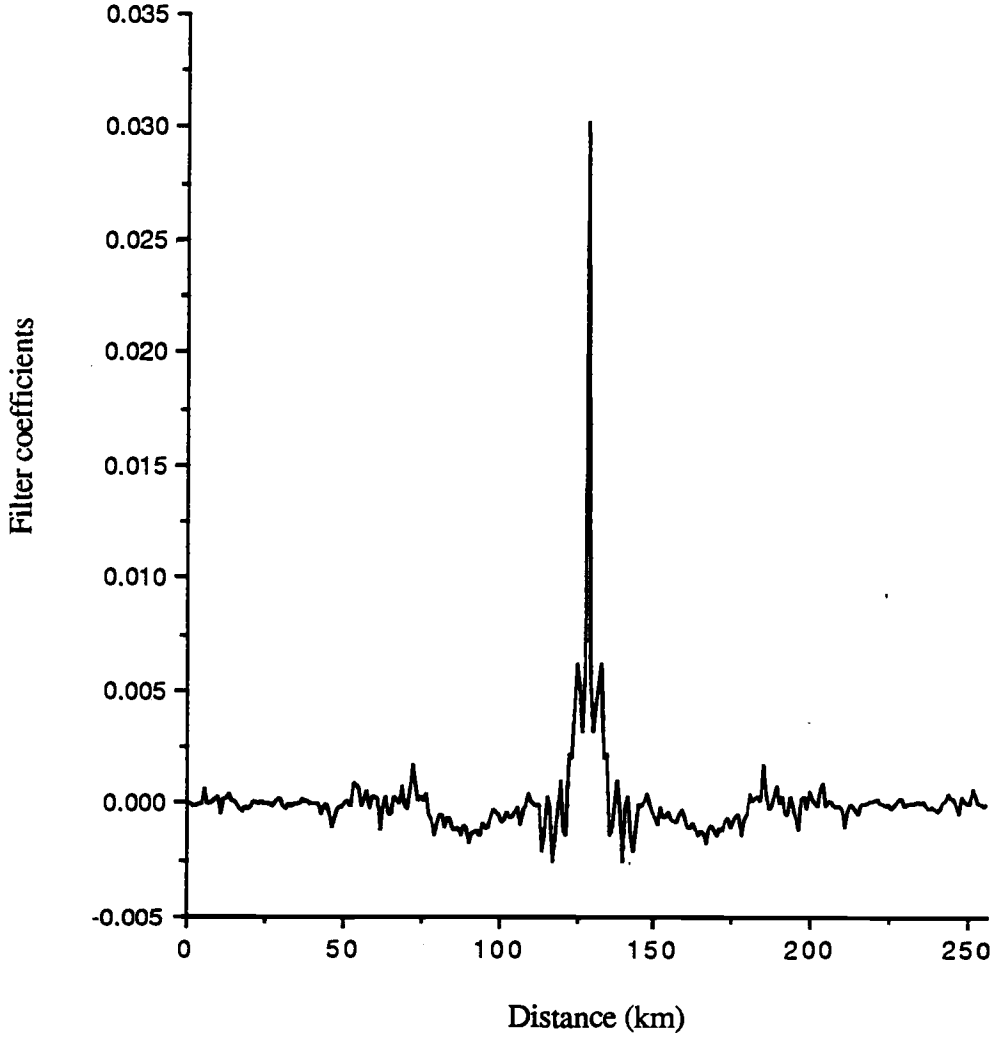

Figure 18 - The admittance filter generated from the 12 gravity and bathymetry profiles shown in figure 12. Space domain representation of figure 17.

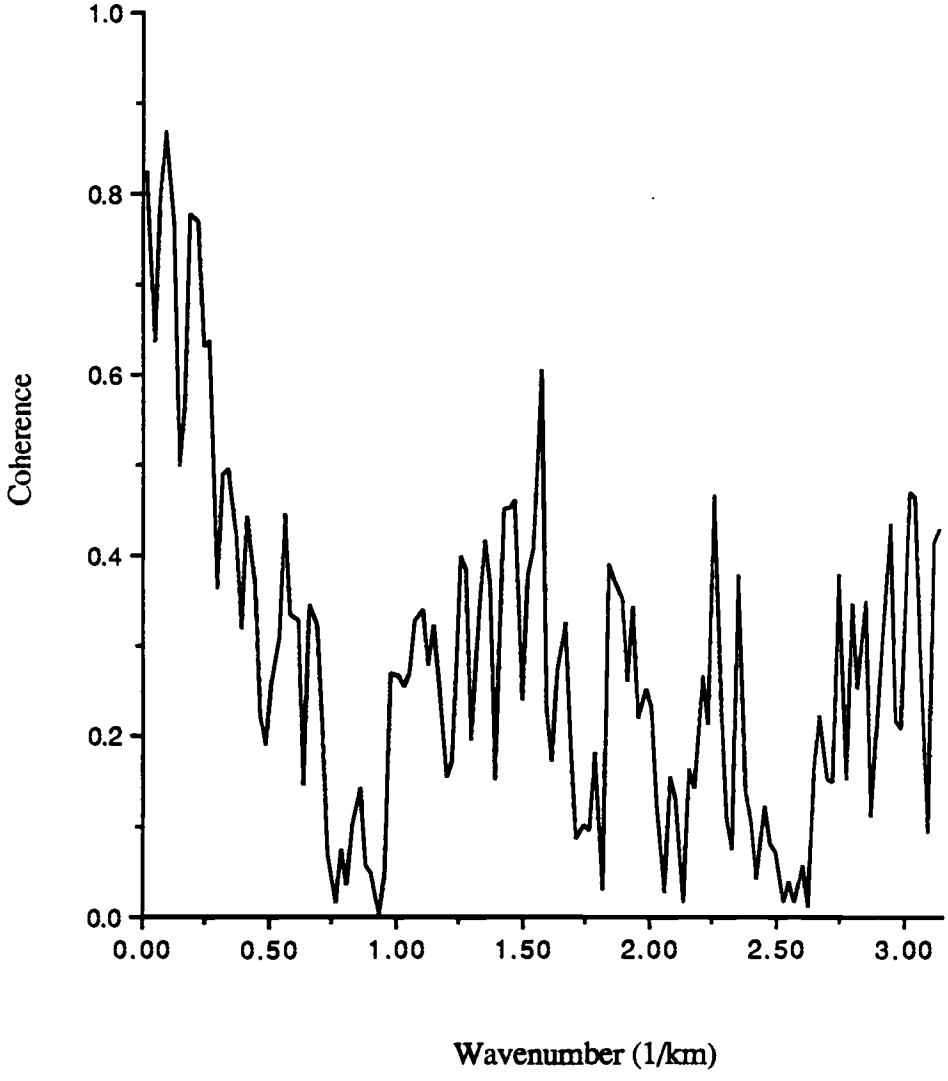

Figure 19 - Coherence plotted against wavenumber

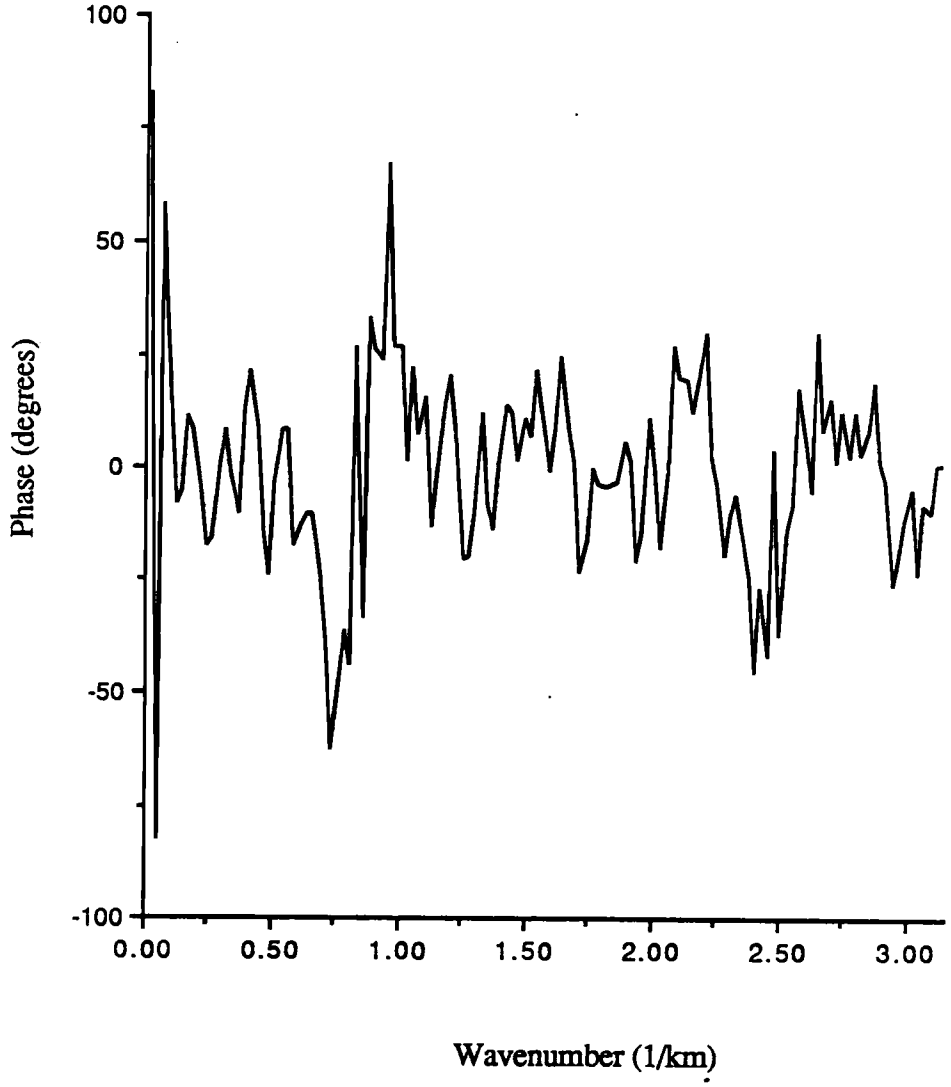

Figure 20 - Phase plotted against wavenumber

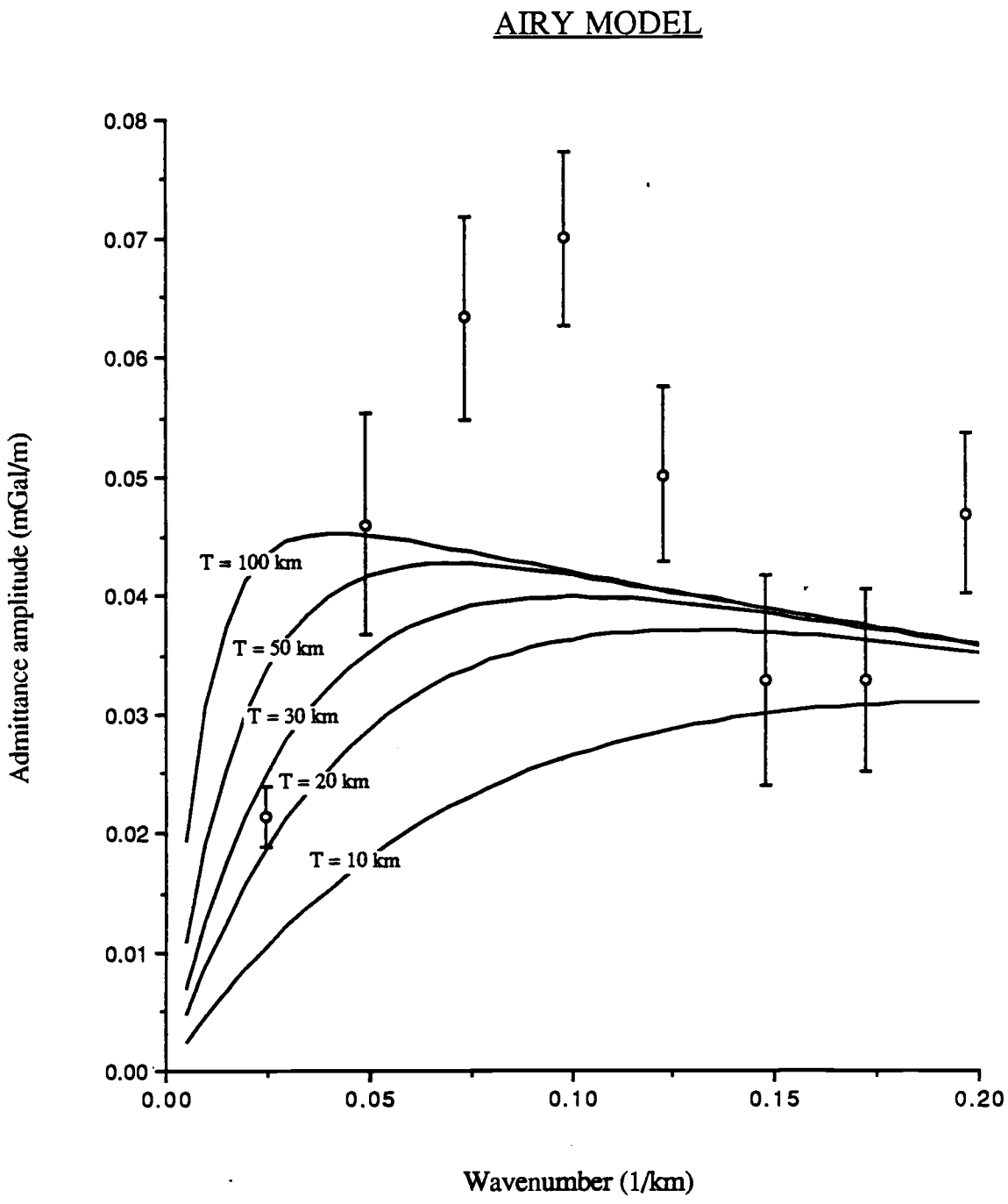

Figure 21 (a) - Experimental admittance estimates (open circles) and theoretical curves for the Airy model (solid lines) for varying values of T (apparent crustal thickness). The vertical bars represent the standard deviation.

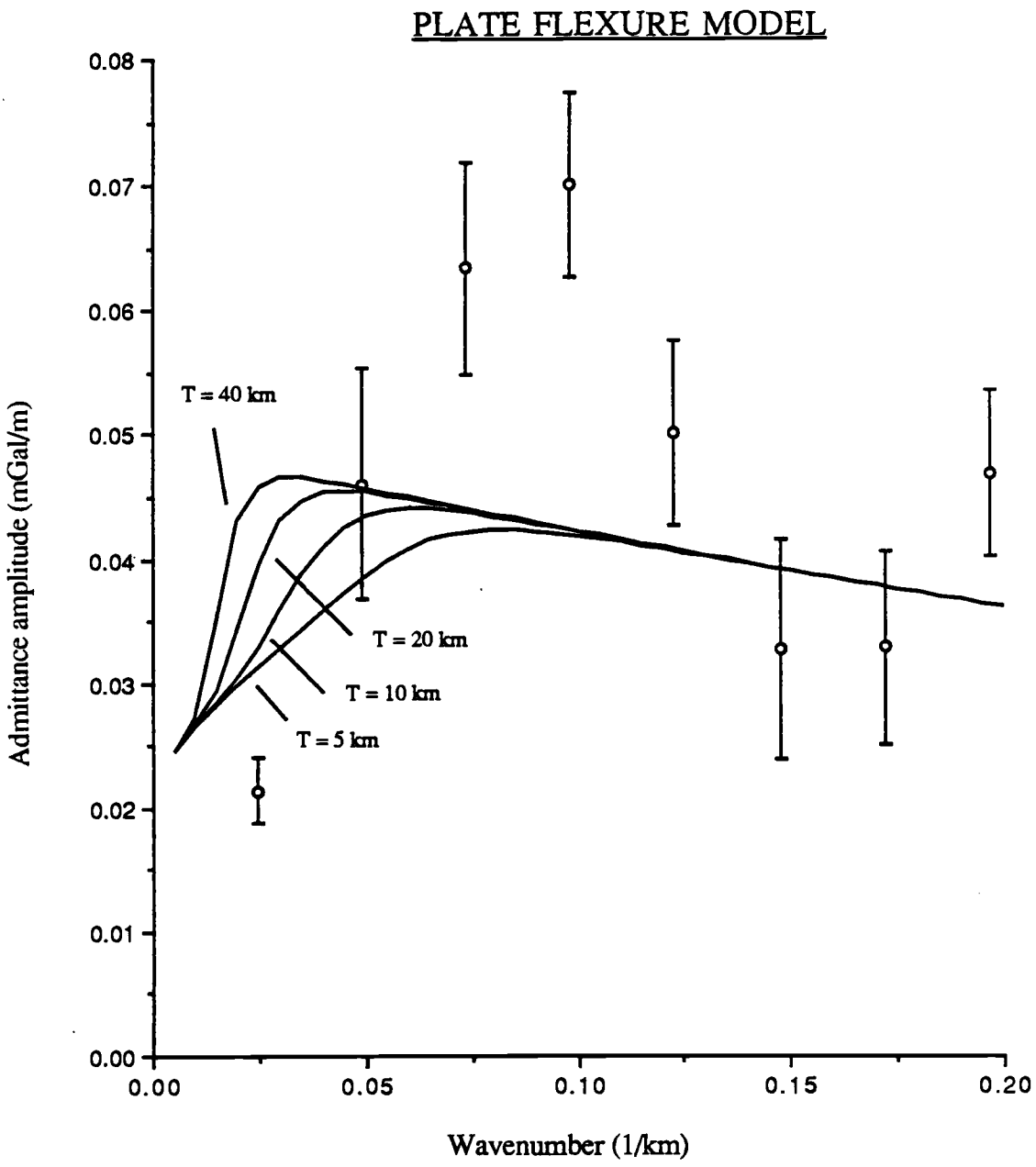

Figure 21 (b) - Experimental admittance estimates (open circles) and theoretical curves for the Plate Flexure model (solid lines) for varying values of T (effective elastic thickness). The vertical bars represent the standard deviation.

TABLE I - Physical parameters used in the admittance analysis

PARAMETER	VALUE
water density (ρ_w)	1030 kgm^{-3}
sediment density (ρ_s)	2200 kgm^{-3}
basement density ($\rho_2 = \rho_c$)	2900 kgm^{-3}
mantle density (ρ_m)	3400 kgm^{-3}
mean water depth (d)	1562 m
gravity acceleration (g)	9.8 ms^{-2}
gravitational constant (g)	6.67 x 10^{-11} Nm^2kg
Young's modulus (E)	10^{11} $kgm^{-1}s^{-2}$
Poisson's ratio (ν)	0.25
Apparent crustal thickness	18,000 m

7 - FORWARD MODELING

Figure 22 shows the cross section obtained by forward modelling the gravity anomaly along profile 6. The location of the modelled gravity signal, orthogonal to the depocenter of the Piaui-Camocim basin, is shown in figure 3. The overall linear structural character of the Brasilian equatorial margin covered in this study justifies the use of a two dimensional line integral algorithm (Talwani et al., 1959) . The gravity along profile 6 consists of a low of -50 mGals over the inner shelf followed by a narrow high of about +40 mGals (30-40 km) at the shelf break and a rather broad low of -30 mGals over the continental rise. The continental shelf extends up to of 100 km from the coastline (indicated by an arrow) and is followed by an 11 degree slope.

The following data constraints have been taken into account when constructing the cross section :

__ Topographic/bathymetric data .

__ Depth to the shallow basement was inferred from seismic reflection line AA' (figure 4). The top of the Parnaiba basement obtained from line AA' was projected normal to the local trend and an average velocity for the sedimentary package of 2.0 km/sec was used to estimate the sediment thickness from the two-way travel time .

__ Two-ship seismic refraction solutions presented by Houtz et al. (1975) (table 2). The midpoint of the seismic refraction profiles have been projected orthogonally onto profile 3. Using their solutions, empirical curves relating P-wave seismic velocities and densities by Ludwig, Nafe and Drake (1957), and assuming no significant lateral changes in density below 50 km, I built an oceanic mass column 50 km thick that fits the observed

free-air gravity anomalies in the area (figure 23). On the premise that the densities of the crustal layers are uniform and equal to those of the mass column , any lateral density departures from that, yields a different gravitational attraction and therefore a non-zero free-air anomaly. The calculated free-air gravity anomaly produced by the two-dimensional model is obtained by subtracting the gravitational attraction of the oceanic column (6467 mGals) from the computed values of the cross section. For a general discussion on the forward modeling procedure using mass columns I refer to Barday (1974). The interactive process of generating the cross section was applied until the least squares misfit between the observed and the calculated values were less than 3 mGals.

The cross-section presented depicts intentionally the simplest model for the crustal structure that fits the gravity data. Unstretched continental crust is shown landward of the hinge zone. The uniform sedimentary infill of the Piaui-Camocim basin is enough to account for the gravity low over the inner shelf and no Moho topography is required. A plausible explanation for this "rootless" basin structure is that the lithosphere is capable of supporting the sediment infill load , and thus has finite flexural rigidity (basin is locally uncompensated).

A sharp transition between continental and oceanic crust is shown in the modelled cross-section. The narrow positive gravity peak over the shelf break requires the slope of the crust/mantle interface to be of the order of 32 degrees. Although the gravity data can be fit assuming a gentler slope, unreasonable density contrasts would be required. Considering the postulated strike/slip and wrenching tectonism during rifting (Zalan and Warm, 1985), the abrupt transition between continental and oceanic lithosphere seems to be reasonable.

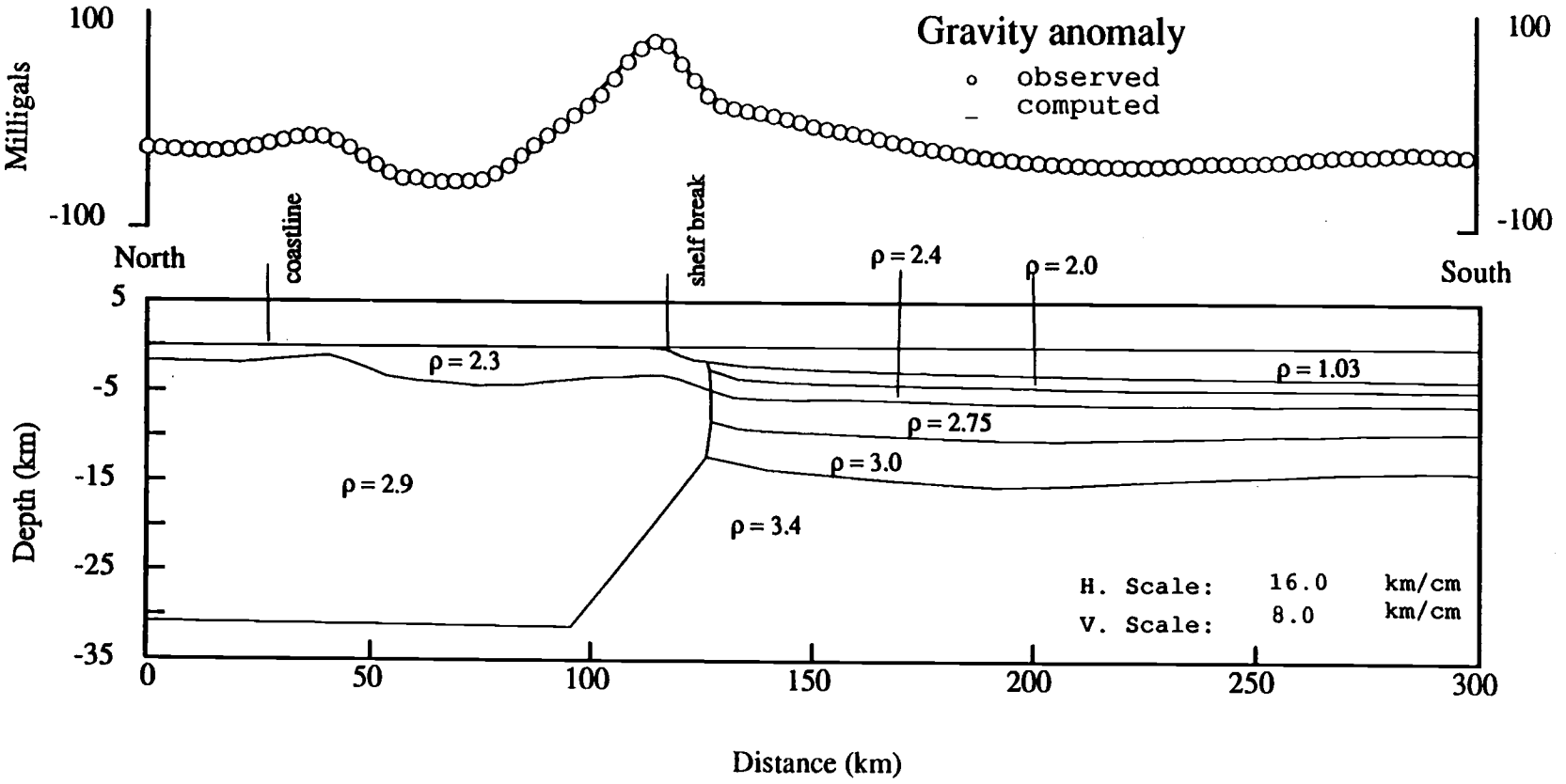

Figure 22 - Crustal model across the equatorial margin of Brazil obtained by forward modelling (2-D line integral method) the gravity anomaly along profile 7 (profile location is shown in figure 9).

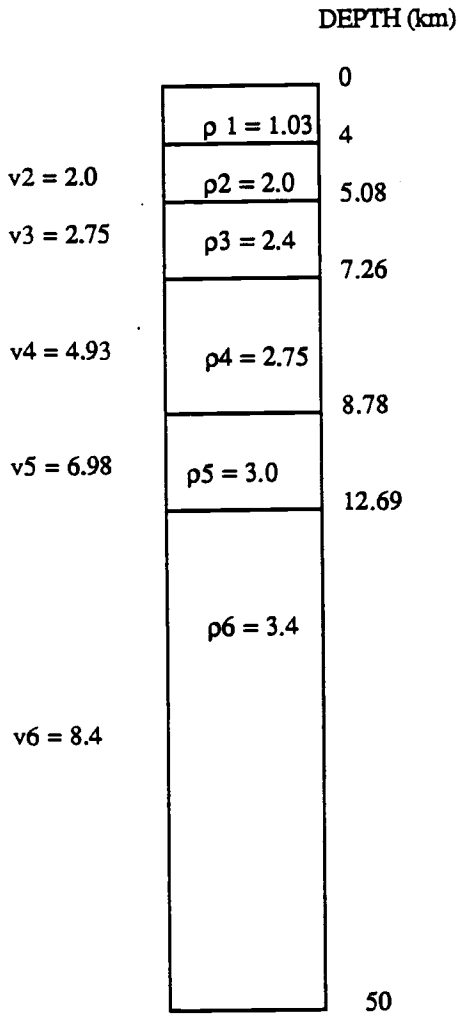

Figure 23 - Calculated mass column from two-ship seismic refraction solutions by Houtz et al. (1977) for R_2.

TABLE II - Two-ship seismic refraction solutions for profile R_2; layer thickness refers to the averaged values between the two shot points

LOCATION : East (00° 38' S and 39° 57' W) - West (00° 21' S and 40° 30' W)

LAYER THICKNESS (km)	VELOCITY (km/sec)	DENSITY (kgm^{-3})
h_1 = 3.80 (water layer)	1.43	1030
h_2 = 1.28 (unconsolidated sediments)	2.00	2000
h_3 = 2.18 (pelagic sediments)	2.75	2400
h_4 = 1.52 (oceanic layer 2)	4.93	2750
h_5 = 3.91 (oceanic layer 3)	6.98	3000
h_6 = 37.31 (mantle)	8.40	3400

8 - SYNTHESIS AND CONCLUSIONS

A large percent of my analysis has addressed the question of finding the most efficient data treatment procedure to minimize truncation effects. After testing several procedures, I concluded that relatively unbiased long-wavelength admittance estimates can be obtained by using the first derivative of the data sets. In addition, it was shown that the mirroring technique, used in previous admittance studies across Atlantic-type margins (Karner and Watts, 1982; Mello and Bender, 1988), leads to an overestimate of the admittance values and, therefore, of the flexural rigidities. Nevertheless, it is still a better choice than the use of tapers.

Figure 18 shows the experimental admittance estimates obtained using the first derivatives of 12 bathymetric and gravimetric profiles. Neither the theoretical curves for the Airy model nor the plate flexure model can explain the experimental admittance estimates . The theoretical curves display a much broader peak than the admittance estimates. Definitely, the long-term mechanical strength of the lithosphere across the equatorial continental margin of Brazil cannot be quantified by using the conventional admittance function approach. This raises the question of the applicability of highly simplified isostatic models for tectonic provinces such as continental margins. I suggest the following explanations to account for the discrepancies between the experimental and theoretical admittance estimates :

(1) The abrupt nature of the transition between oceanic and continental crust controlled by the Romanche Fracture Zone - Unlike the eastern North American continental margin which was formed as result of extensive rifting and pulling appart, the obliquely-rifted equatorial margin of Brazil has undergone a complex tectonic evolutionary process,

where additional components such as shear and right-lateral wrenching were present . Although the nature and extent of the transition between oceanic and continental crust for this study area is still not well known, it probably occurs over a much narrower zone than most of the U.S. Atlantic margin, where the continental lithosphere has been significantly stretched. Therefore, representing the margin as a thin homogeneous elastic plate might be reasonable when the transition is gradual (for which the uniform flexural rigidity assumption seems reasonable) but is probably not a good approximation when it is as abrupt as the equatorial margin of Brazil .

(2) Presence of subsurface load - Estimates of the average flexural rigidity on margins using the conventional admittance approach are obviously biased when buried or subsurface loads (located within or beneath the plate) are present instead of superficial loads (McNutt, 1983; Forsyth, 1985). According to Forsyth (1985), when surface and subsurface loads are present and/or provinces with distinct mechanical behaviour are averaged together, the flexural rigidity estimates are systematically biased toward low values. In the context of passive margins, large apperture seismic data supports the existence of thick lens of high velocity lower crustal material beneath the Caroline Trough (Trehu et al., 1988) which can be interpreted as a source of subsurface loading. Lithospheric thermal anomalies and compositional variations at large depths represent additional sources of subsurface loading as well as any marked variations in density at shalower depths (e.g. sediementary basins). In principle, the proximity of the Romanche Fracture Zone (bounding the study area to the north) and associated volcanism suggest that buried loads, represented by intrusive bodies, might be present in the area. Forsyth (1985) showed that , if surface and subsurface loading are statiscally independent or uncorrelated, unbiased estimates of the flexural rigidity of the lithosphere can be obtained by analysis of the wavelength of transition between coherent and incoherent wavebands instead of using

the admittance. However, the use of Forsyth's approach requires extending the study area to the north (seawards) and south (landwards) for which data is not available (on land).

(3) "Masked" estimates - The admittance estimates presented here are likely to reflect the combination of two different signals : one related to the compensation of the Barreirinhas/Piaui-Camocim sub-basin which has no topographic/bathymetric expression and the other one related to the topography/bathymetry and its compensation which is of interest in the admittance studies. Since the wavelengths of these signals do not differ by much (around 80-100 km for the basin) it is possible that in the averaging process some overlaping occurs. The combination of these signals could yield anomalous results masking the admittance estimates in the diagnostic waveband.

10 - BIBLIOGRAPHY

Azevedo, R.P., 1986, Interpretacao geodinamica da evolucao mesozoica da bacia de Barreirinhas: Anais do XXXIV Congresso Brasileiro de Geologia, Goiania, Goias, v.3, p. 1115-1130.

Banks, R.J., R.L. Parker and S.P. Huetsis, 1977, Isostatic compensation on a continental scale, Geophys. J. R. astr. Soc., 51, p. 431-452.

Barday, R.J., 1974, Structure of the Panama basin from marine gravity data: M.S. Thesis, Oregon State University, Corvallis, Oregon, 99 p.

Briggs, I.C., 1974, Machine contouring using minimum curvature: Geophysics, v. 39, no. 1, p. 39-48.

Cochran, J.R., 1973, Gravity and magnetic investigations in the Guiana basin, Western Equatorial Atlantic: Geolog. Soc. Amer. Bull., v. 84, p. 3249-3268.

Cochran, J.R., 1980, Some remarks on isostasy and the long-term behaviour of the continental lithosphere: Earth and Planetary Science Letters, 46, p. 266-274.

Costa, M.P.A. and R.O. Kowsmann, 1981, Tectonismo vertical no pos-Paleogeno do PLato de Ceara e suas possiveis causas e implicacoes: Bull. Tec. Petrobras, 24(1), p. 23-32.

Dehlinger, P., 1978, Marine Gravity: Elsevier Oceanography Series, No. 22, Elsevier Scientific Publishing Company, New York, 322 p.

Diament, M, 1985, Influence of method of data analysis on admittance computation: Annales Geophysicae, 3, 6, p. 785-792.

Diament, M., J.C. Sibuet and A. Hadaoui, 1986, Isostasy of the Northern Bay of Biscay continental margin: Geophys. J.R. astr. Soc., v. 86, p. 893-907.

Dorman, L.M. and B.T R. Lewis, 1970, Experimental isostasy 1. Theory of the determination of the earth's isostatic response to a concentrated load: J. Geophys. Res., v.75,, no. 17, p. 3357-3365.

Forsyth, D.W., 1985, Subsurface loading and estimates of the flexural rigidity of continental lithosphere: J. Geophys. Res., v. 90, no. B14, p. 12,623-12,632.

Forsythe, G.E., M.A. Malcolm, C.B. Moler, 1977, Computer methods for mathematical computations: Prentice-Hall Inc, 77 p.

Francolin, J.B.L. and P. Szatmari, 1987, Mecanismo de rifteamento da porcao oriental da margem norte brasileira: Revista Brasileira de Geociencias, 17(2), p. 196-207.

Gorini, M.A., 1981, The tectonic fabric of the equatorial Atlantic and adjoining continental margins: Gulf of Guinea to northeastern Brazil: Projeto Remac, v. 9, p. 11-116.

Houtz, R.E., W.J. Ludwig, J.D. Miliiman and J.A. Grow, 1977, Structure of the northern Brazilian continental margin: Geol. Soc. Am. Bull., v. 88, p. 711-719.

Jeffreys, H., 1976, The Earth: Cambridge University Press, New York, 438 pp.

Karner, G.D. and A.B. Watts, 1982, On isostasy at Atlantic-type continental margins: J. Geophys.Res., v. 87, n0. B4, p. 2923-2948.

LePichon, X. and D.E.Hayes, 1971, Marginal offsets, fracture zones and the early opening of the South Atlantic: J. Geophys. Res, v. 76, p. 6283-6293.

Lobo, A.P., 1987, Evidencia sismica da zona de fratura de Romanche, a sub-divisao de crosta no sope continental das bacias de Potiguar e do Ceara e sua implicacao na exploracao do petroleo, Internal Report, Petrobras, Depex-Dirnoe-Sercepo, 36 p.

Louden, K.E., 1981, A comparison of the isostatic response of the bathymetric features in the north Pacific Ocean and Philippine Sea, Geophys. J. R. astr. Soc., 64, p. 393-424.

Louden, K.E. and D.W. Forsyth, 1982, Crustal structure and isostatic compensation near the Kane fracture zone from topography and gravity measurements - I. Spectral analysis approach: Geophys. J. R. astr. Soc., 68, p. 725-750.

Mello, U.T. and A A. Bender, 1988, On isostasy at the Equatorial Margin of Brazil: Revista Brasileira de Geociencias, 18(3), p. 237-246.

McKensie, D.P. and C. Bowin, 1976, The realtionship between bathymetry and gravity in the Atlantic ocean: J. Geophys. Res., v. 81, p. 1903-1915.

McNutt, M.K.,1983, Influence of plate subduction on isotatic compensation in Northern California: Tectonics, v. 2, no. 4, p. 399-415.

Miura, K and J.C. Barbosa, Geologia da plataforma continental do Maranhao, Piaui, Ceara e Rio Grande do Norte, 1972: Congresso Brasileiro de Geologia, 26, Belem, Anais XXVI Congresso Brasileiro de Geologia, Sao Paulo, Sociedade Brasileira de Geologia, v.2, 57-66.

Munk, W.H. and D.E. Cartwright, 1966, Tidal spectroscopy and prediction: Phyl. trans. Roy. Soc., 31, p. 447-455

Parker, R.L., 1972, The rapid calculation of potential anomalies: Geophys. J. R. astr. Soc., 31, p. 447-455.

Parsons, B. and J.G. Sclater, 1977, An analysis of the variation of ocean floor bathymetry and heat flow with age: J. Geophys. Res., v. 82, no. 5, p.803-827.

Rapp, R.H., 1986, Gravity anomalies and sea surface heights derived from a combined GEOS 3/SEASAT altimeter data set: J. Geophys. Res., v. 91, no. B5, p. 4867-4876.

Reamer, S.K. and J.F. Ferguson, 1989, Regularized two-dimensional Fourier gravity inversion method with application to the Silent Canyon caldera, Nevada: Geophysics, v.54, no. 4, p. 486-496.

Ribe, N.M., 1982, On the interpretation of frequency response functions for oceanic gravity and bathymetry: Geophys. J. R. astr. Soc., 70, p. 273-294.

Ribe, N.B. and A.B. Watts, 1982, The distribution of intraplate volcanism in the Pacific Ocean basin: aspectral approach, Geophys. J. R. astr. Soc., 71, p.333-362.

Spector, A. and F.S. Grant, 1970, Statistical model for interpreting aeromagnetic data: Geophysics 35, p. 293-302.

Szatmari, P., J.P.L. Francolin, O. Zanotto and S. Wolf, 1987, Evolucao tectonica da margem equatorial brasileira: Rev. Bras. Geoc., 17(2), p. 180-188.

Talwani, M., J.L. Worzel, and M. Lindisman, 1959, Rapid gravity computation for two-dimensional bodies with application to the Mendocino submarine fracture zone: J. Geophys. Res., v. 64(1), p. 49-59.

Thorne, J.A. and A.B. Watts, 1989, Quantitative analysis of North Sea subsidence: AAPG Bul., v. 73, No 1, p. 88-116.

Tikhonov, A.N., V.B Glasko, O.R. Litvinenko, and V. Melikhov, 1968, Analytic continuation of a potential in the direction of the disturbing masses by the regularization method: Izv., Earth Physics, 12, p. 30-48.

Trehu, A.M., A. Ballard, L.M. Dorman, J.F. Gettrust, K.D. Klitgord and A. Schreiner, 1988, Structure of the lower crust beneath the Caroline Trough, U.S. Atlantic Continental Margin: J.Geophys. Res., in press.

Turcotte, D.L., 1979, Flexure: Advances in Geophysics, v. 21, Academic Press,p. 51-85.

Turcotte, D.L. and G. Schubert, 1982, Geodynamics: Applications of Continiuum Physics to Geological Problems, John Wiley & Sons, New York, 450 pp.

Young, R. and I.A. Hill, 1986, An estimate of the effective elastic thickness of the Cape Verde Rise, J. Geophys. Res., v. 91, no. B5, p. 4854-4866.

Watts, A.B., 1978, An analysis of isostasy in the world's ocean, 1, Hawaian-Emperor seamount chain: J. Geophys. Res., 83, p. 5989-5004.

Watts, A.B., 1988, Gravity anomalies, crustal structure and flexure of the lithpsphere at the Baltimore Canyon Trough, 1988: Earth and Planet. Sci. Let., 89, p. 221-238.

Watts, A.B., J.H. Bodine and M.S. Steckler, 1980, Observations of flexure and the state of stress in the ocean lithosphere, J. Geophys. Res., v. 85, p. 6369-6376.

Watts, A.B., 1981, The U.S. Atlantic continental margin: subsidence history, crustal structure, and thermal evolution: Geology of passive Continetal Margins: History, Structure and Sedimentological Record (with special emphasis on the Atlantic margin), AAPG education course note series, 19, p. 2-to -2-75.

Watts, A.B. and J. Thorne ,1984, Tectonics, global changes in sea-level and other relationship to stratigraphical sequences at the U.S. Atlantic continental margin: Marine and Petrloleum Geology, 1, p. 319-339.

Zalan, P.V. and J.E. Warne, 1985, Tectonics and sedimentation of the Piaui-Camocim sub-Basin, Ceara Basin, offshore northeastern Brazil: Bol. Geociencia Tecnica-Petroleo, v. 17, 71 p.

APPENDICES

APPENDIX A

DOWNWARD CONTINUATION

The question of whether or not there is any evidence for the presence of buried loads can be addressed in a different way, by obtaining the crust-mantle relief. The approach that I use consists of convolving a theoretical admittance function z(x), assuming local compensation (expression 29), with the bathymetry b(x) (profile 7) producing the "predicted" gravity anomaly $g_p(x)$.

Figure A1 shows some of the several values tried for the apparent crustal thickness (T_{ca}). In a least squares sense, the best fit to the edge-effect high occurs for $T_{ca} = 18$ km. The difference between the "predicted" gravity anomaly, for $T_{ca} = 18$ km, and the observed gravity anomaly yields the residual isostatic gravity anomaly shown in figure A2. In principle, this residual anomaly only contains the short-wavelength components of the observed gravity anomaly, since the regional anomaly related to the bathymetry and its compensation has been removed. Note that the high-frequency content of the observed gravity anomaly (eg. the edge-effect high) is not completely reproduced by the "predicted" anomaly. The observed differences at this inflection point are related to the errors introduced by using a linear isostatic model (neglecting high order terms in expressions (19) and (20).

Before applying the FFT, the mean of the residual isostatic anomaly was removed and a 10% cosine taper was applied to both ends. The downward continuation of the residual isostatic gravity anomaly $\Delta g(k_n)$ (in the Fourier domain) to a depth z_m yields the crust-mantle relief $\Delta R(k_n)$:

$$\Delta R\,(k_n) = \frac{\Delta g\,(k_n)\exp\,(k_n Z_m)}{2\,\pi\,\gamma\,(\rho_m - \rho_c)} \qquad (a_1)$$

The use of the downward continuation operator exp (k z_m) yields highly unstable results as short-wavelength white noise, due to either shallow mass distribution and/or observational errors are significantly amplified above the signal level. Low- pass filters are commonly applied to the data in an attempt to yield stable results. However, overfiltering or underfiltering can occur if the filter does not take into account the spectral characteristics of the data. In this study, I use the regularization filter (Tikhonov et al., 1968) which tapers the downward continuation operator at high-wavenumbers and has an almost negligible effect at small wavenumbers.

$$f\,(k,\alpha,z_m) = \frac{1}{1 + \alpha\,k\exp\,(kz_m)} \qquad (a_2)$$

The alpha parameter (α) controls the decay rate of the regularization filter as the wavenumber increases. It is important to find an optimal value for alpha which controls the growth of the downward continuation operator without leading to overfiltering or underfiltering. This optimal value is, in turn, dependant on the spectral characteristics of the data, specifically the crossover wavenumber k_c. This is the wavenumber that separates signal from noise and occurs at a point where the the signal-to-noise ratio is assumed to be equal to one (figure B1 - appendix B). The low-wavenumber portion of the spectrum contains the signal or source information.

Spector and Grant (1970) have shown that the slopes of the line segments are directly proportional to the depth of the sources. This study assumes that the low wavenumber part of the spectrum is dominated by only one deep source at a depth z_m, that is the crust-mantle interface. For higher wavenumbers the power spectrum becomes "flat"

and is attributed to the presence of shallower sources and white noise. Not only is this noisy portion of the signal of no interest in this study but it is also significantly amplified in the downward continuation process. Finding the crossover wavenumber is important, since I seek a regularization filter which will retain the maximum amount of source information with a minimum amount of noise.

Figure A3 shows the power spectrum of the residual gravity anomaly which is approximated by two linear splines : one represented by a sloping segment for the low-wavenumber portion, which contains the signal, and another one as a flat segment for the high-wavenumber portion dominated by noise (appendix B). Both linear splines must satisfy the following conditions : they must intersect at the crossover wavenumber and the second spline must have a zero slope. The next step consists of finding the minimum value for the summed squared misfit (error) between the spectral estimates, partitioned at k_c, and the linear splines. The summed squared misfit calculated for different values of k_c is shown in figure B2 (appendix B) and the optimal k_c occurs at the inflection point . The optimal value for the crossover wavenumber of the residual isostatic gravity spectrum is : 0.785 km^{-1}. I then used the following empirical relationships derived, by Reamer and Ferguson (1989), that relates k_c, alpha and the continuation depth z_m :

$$\log_{10}(\alpha) = \log_{10}(\alpha_o) + S\, k_c \qquad (a_3)$$

$$S = -0.623 - 0.583\, z_m \qquad (a_4)$$

$$\log_{10}(\alpha_o) = 0.303 + 1.928 \log_{10}(z_m) \qquad (a_5)$$

In a typical Atlantic-type continental margin, the depth to the Moho is estimated to range from 40-50 km at the shoreline to as shallow as 9-12 km in deep waters. Since the downward continuation depth should not exceed 0.9 times the source depth (Reamer and Ferguson, 1989), the deepest continuation depth should not be greater than 5.4 km (the

sediment infill of the Piaui-Camocim basin is estimated to be of the order of 6 km). Figure A4 shows the regularized downward continuation of the residual isostatic anomaly, for z_m=5.4 km,modelled as the relief on the crust-mantle interface. Note that the high frequency content in the residual isostatic anomaly was obviously amplified in the process. According to figure A4, substantial variations in the crust/mantle relief, of the order of 1.5 km, are required beneath Piaui-Camocim basin, which can be interpreted as evidence for crustal thickening. However, it is important to recognize that a major portion of the residual isostatic anomaly low is exclusively related to density variations within the crust (sediment infill). Unfortunately, since the true basin depth and geometry is not known, it becomes impossible to isolate the part of the signal due to density variations from the part due to changes in crustal thickness.

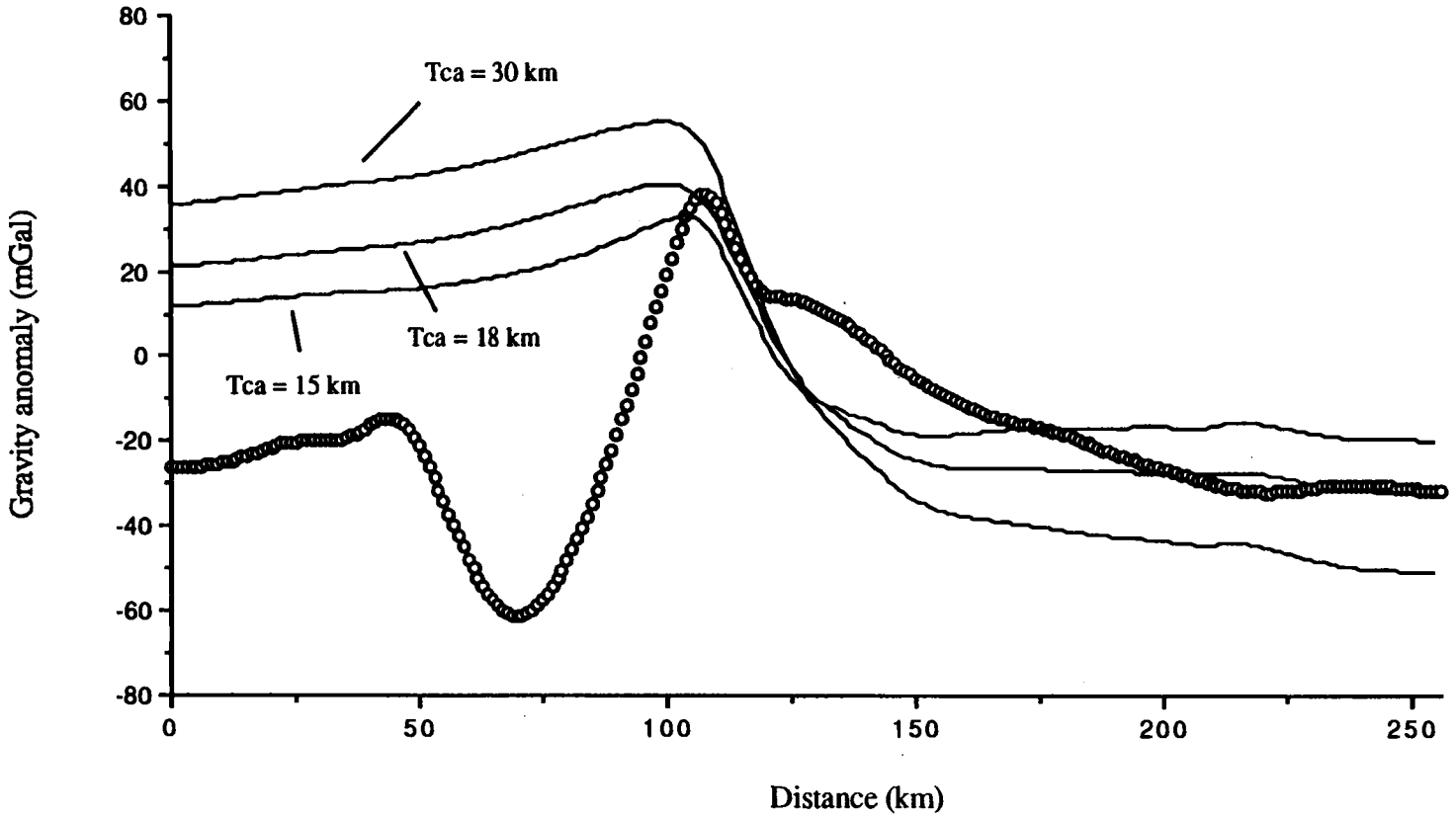

Figure A1 - Observed gravity along profile 7 (open circle) and "predicted" gravity anomaly for the Airy model for varying apparent crustal thickness. The best fit occurs for Tca = 18 km.

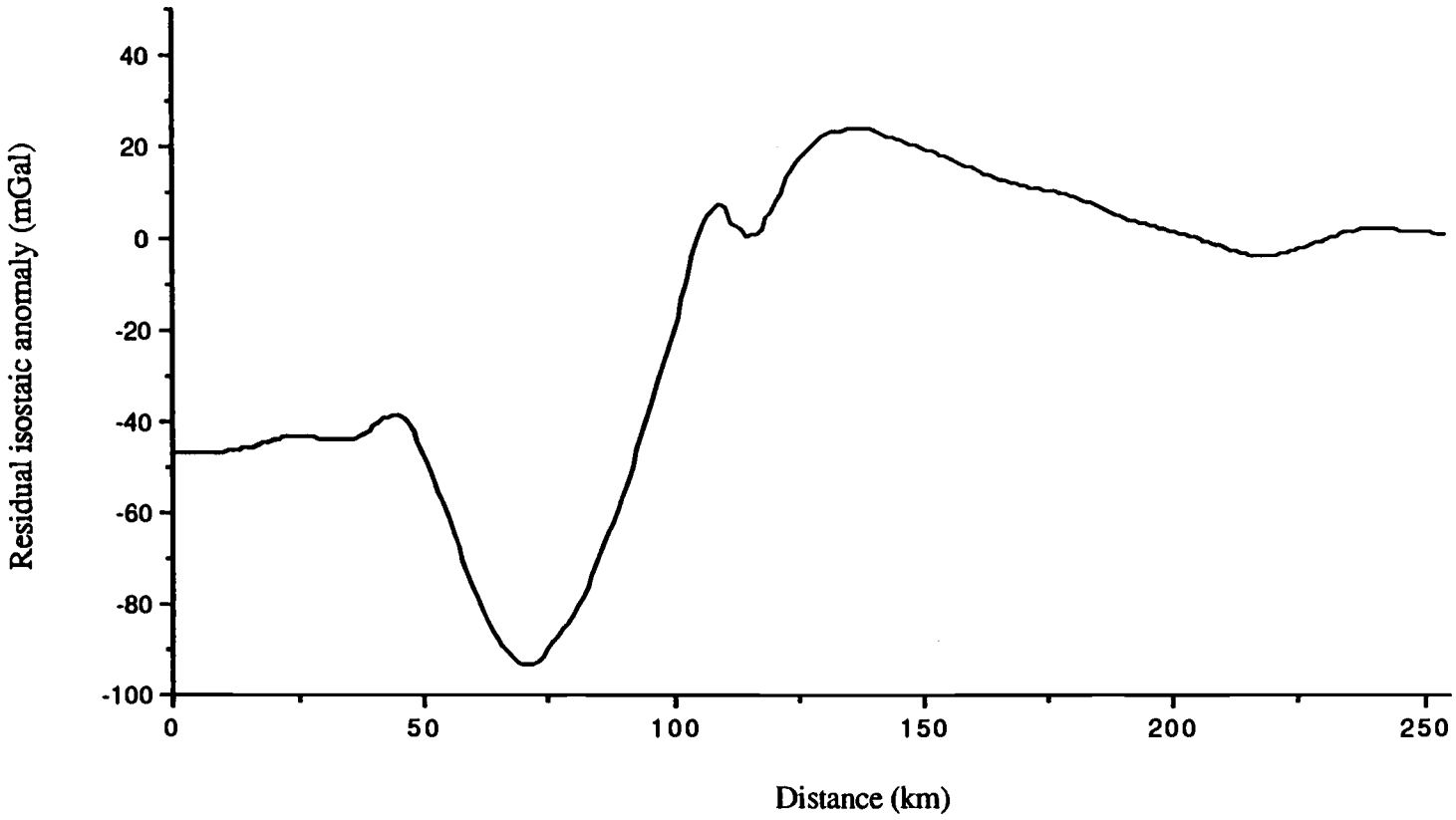

Figure A2 - Residual isostatic anomaly (assuming Airy isostasy) obtainned by subtracting the "predicted" anomaly from the observed.

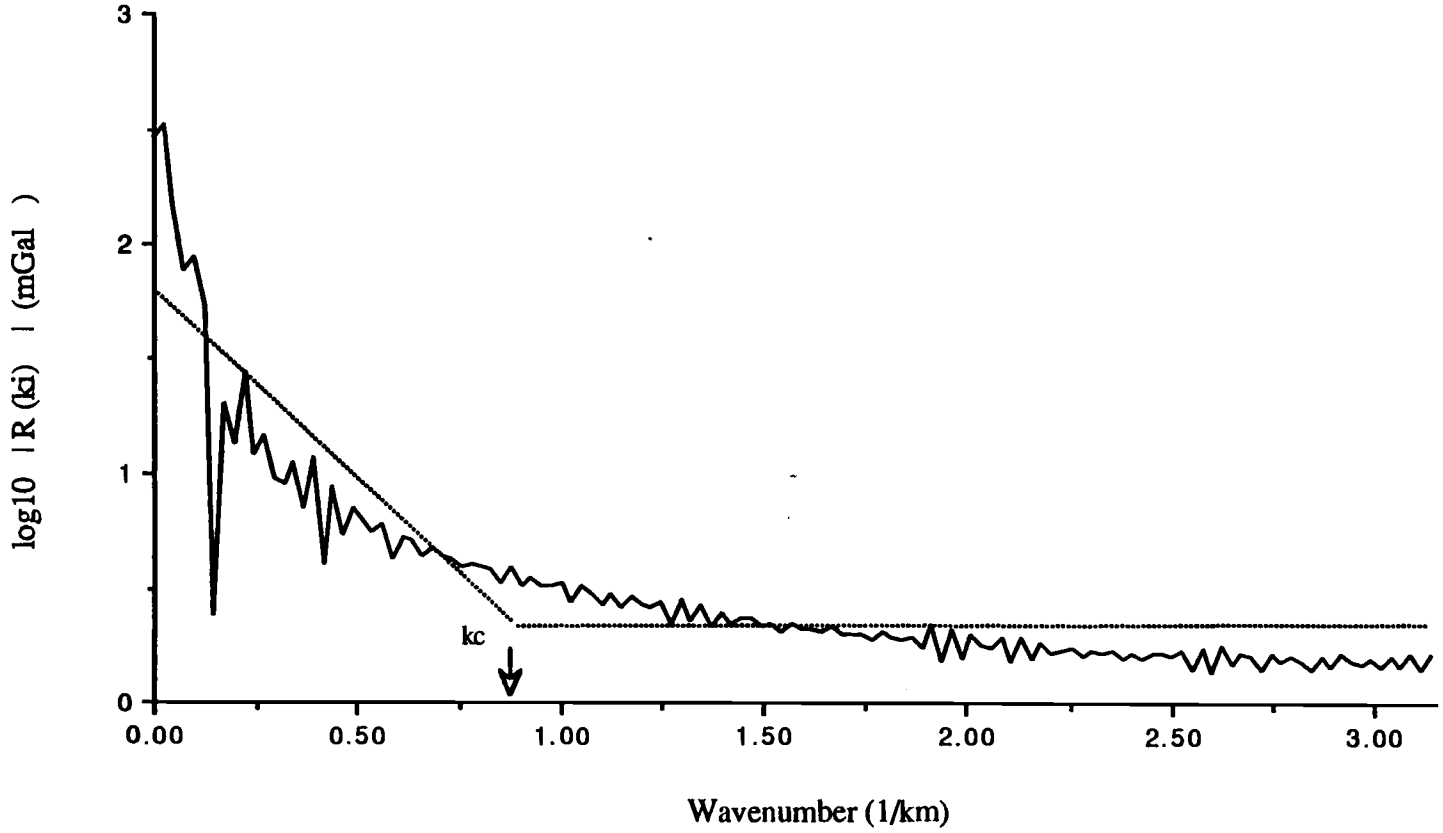

Figure A3 - Power spectrum of the residual isostatic anomaly shown in figure 23. Dotted line indicates the power spectrum estimates fit, on a least squares sense, to two linear linear splines crossing at kc.

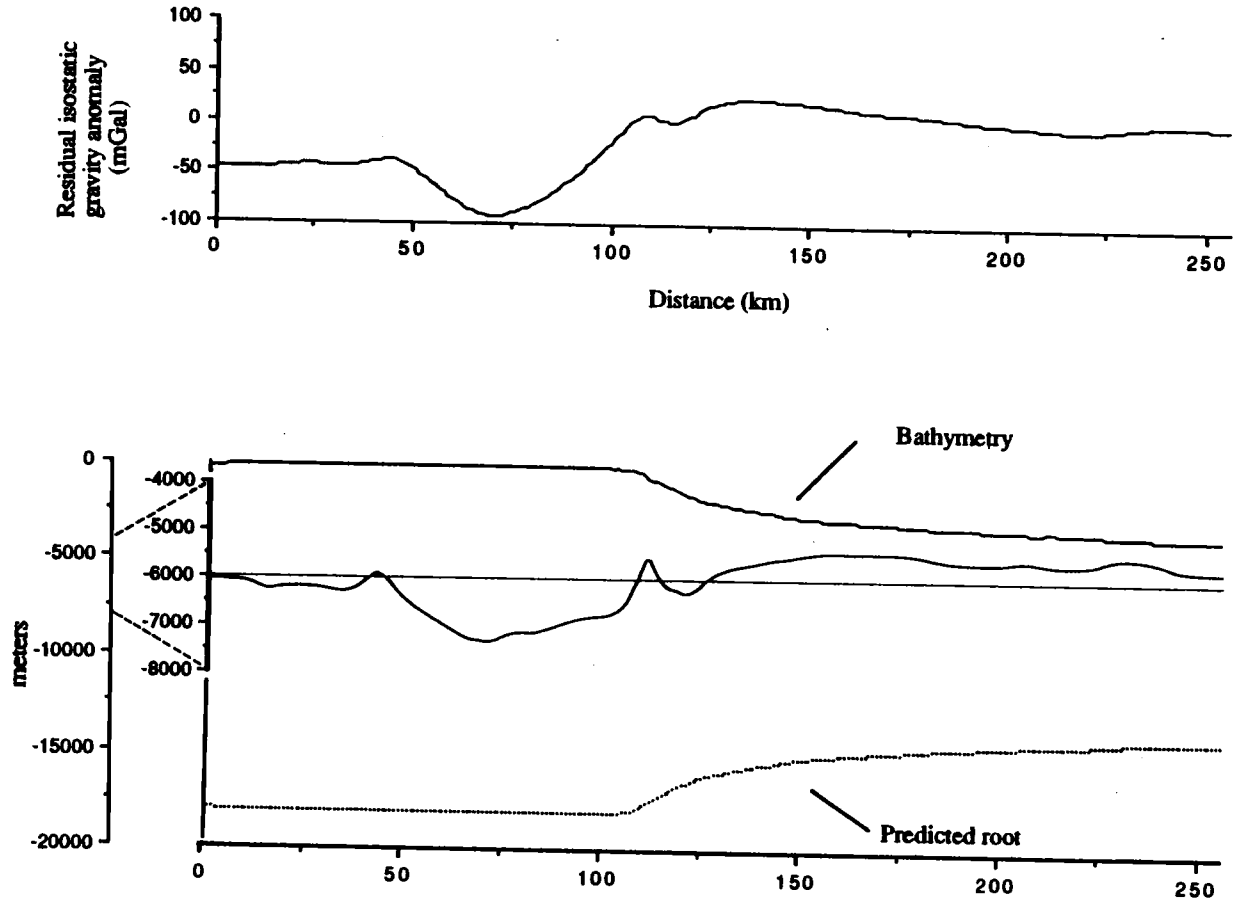

Figure A4 - The residual isostatic gravity anomaly was obtained by subtracting the "predicted" anomaly for T_{ca} = 18 km from the observed. The regularized downward continuation of this anomaly (for z_m = 5.4 km) yields the crust-mantle relief . Dotted line indicates the predicted root assuming point-to-point Airy type of compensation.

APPENDIX B

DETERMINATION OF THE CROSS-OVER WAVENUMBER

Figure B1 shows the power spectral estimates (N data points (k_i, $P(k_i)$), i = 0,1,2... 128) partitioned at the crossover wavenumber k_c. We want to find the crossover wavenumber k_c such that for $k_i < k_c$ the spectral estimates fit, in a least squares sense, the straight-line model $y = a + bk_i$ and for $k_i > k_c$ the model $y = a + bk_c$. This constrains both solutions to merge at k_c and the noise portion of the spectrum to have zero slope. The model parameters a and b are determined, in a least squares sense, by minimizing the summed squared error (δ_i^2) between the spectral estimates and the straight-line models :

$$E = \sum_{i=0}^{Nyquist} (\delta (k_i))^2 \qquad (b_1)$$

Since the spectral estimates are partitioned at k_c such that for $0 \le k_i \le k_c$ we have n_1 samples and for $k_{Nyquist} \le k_i < k_c$ we have n_2 samples ($N = n_1 + n_2$) we can write (b_1) as:

$$E = \sum_{i=0}^{c} | P(k_i) - (a + bk_i) |^2 + \sum_{i=c+1}^{Nyquist} | P(k_i) - (a + bk_c) |^2 \qquad (b_2)$$

where :

E - summed squared error

$P(k_i)$ = log10 of the power spectrum (log10 | $R(k_i)$ |)

$k_i = i\,(2\pi)/256 \qquad i = 0,1,2 \ldots 128$

$k_{Nyquist}$ = Nyquist frequency ($= \pi$ in this study)

a, b - straight-line model parameters corresponding to the

T- intercept and slope respectively

Note that when the values of $P(k_i)$ are thought to be of unequal reliability or precision, we can modify expression (b_1) to include a positive weight factor w(ki) which represents a measure of the degree of precision or relative importance of the value $P(k_i)$:

$$E = \sum_{i=0}^{Nyquist} w(k_i)\ \delta_i^2 \qquad (b_3)$$

The minimization of expression (b_2) is accomplished by setting the partial derivatives in terms of a and b to zero as shown:

$$\frac{\delta E}{\delta a} = \sum_{i=0}^{c} -2\ |\ P(k_i) - (a + bk_i)\ | \ + \sum_{i=c+1}^{Nyquist} -2\ |P(k_i) - (a + bk_c)\ | \qquad (b_4)$$

$$\frac{\delta E}{\delta b} = \sum_{i=0}^{c} -2\,k_i\ |\ P(k_i) - (a + bk_i)\ | \ + \sum_{i=c+1}^{Nyquist} -2\,k_c\ |P(k_i) - (a + bk_c)\ | \qquad (b_5)$$

Rewriting expressions (b_4) and (b_5) it follows that :

$$0 = \sum_{i=0}^{c} P(k_i) - b\sum_{i=0}^{c} k_i - n_1 a + \sum_{i=c+1}^{Nyquist} P(k_i) - n_2 a - n_2 b\,k_c$$

$$(b_6)$$

$$0 = \sum_{i=0}^{c} P(k_i)\,k_i - a\sum_{i=0}^{c} k_i - b\sum_{i=0}^{c} k_i^2 + k_c \sum_{i=c+1}^{Nyquist} P(k_i) - n_2 a k_c - n_2 b k_c^2$$

$$(b_7)$$

In matrix form :

$$\begin{pmatrix} \sum_{i=0}^{c} P(k_i) + \sum_{i=c+1}^{nyquist} P(k_i) \\ \sum_{i=0}^{c} P(k_i)\,k_i + k_c \sum_{i=c+1}^{nyquist} P(k_i) \end{pmatrix}$$

$$= \begin{pmatrix} n_1 + n_2 & \sum_{i=0}^{c} k_i + k_c n_2 \\ \sum_{i=0}^{c} k_i + k_c n_2 & \sum_{i=0}^{c} k_i^2 + k_c^2 n_2 \end{pmatrix} \begin{pmatrix} a \\ b \end{pmatrix}$$

The solution to this linear system gives the straight-line parameters satisfying the initial conditions imposed for a given initial guess of k_c. Once a and b are obtained we can calculate the summed squared error from expression (b_2) and repeat the same procedure for several values of k_c. Figure B2 shows the summed squared error values for varying values of k_c (these estimates were made for the power spectrum of the residual isostatic anomaly shown in figure A3). The solid line indicates the fifth order polynomial that best approximates these estimates. The optimal k_c occurs at the inflexion point of this curve and can therefore be found by finding the minimum of the polynomial (where its first derivative is zero). An optimization procedure (Forsythe et al.,1977), based on the combination of

parabolic interpolation and golden-section search (subroutine FMIN) is used. The optimal value for k_c found is 0.785 km^{-1} .

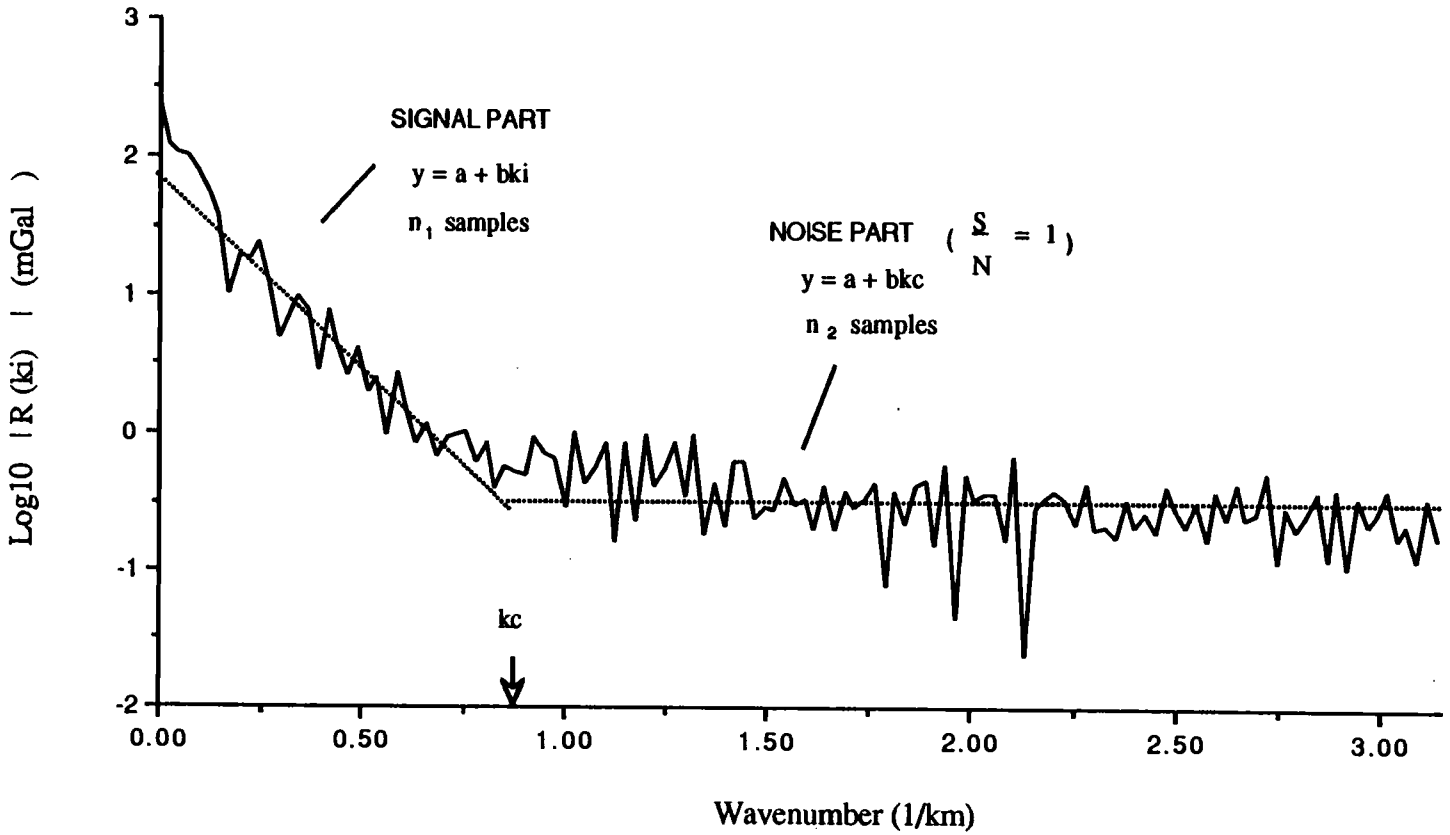

Figure B1 - Example of power spectrum estimates fit, on a least squares sense, to a straight-line model shown as two dotted lines crossing at kc.

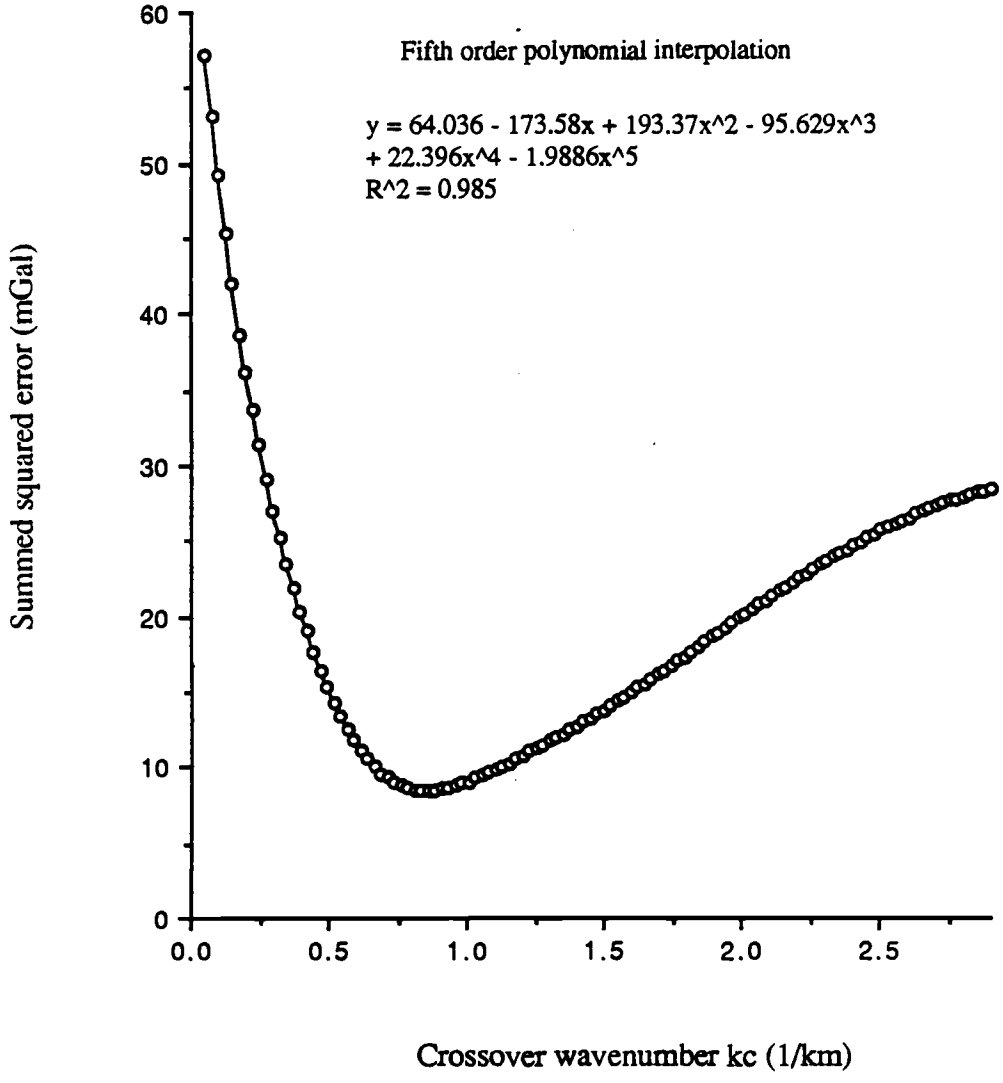

Figure B2 - Estimates (open circles) for the summed squared error plotted for varying values of kc; solid line indicates the 5th order polynomial interpolation.